Geol. Mag. **140** (*4*), *2003, pp. 373–395.* © *2003 Cambridge University Press*
DOI: 10.1017/S001675680300801X *Printed in the United Kingdom*

Neoproterozoic evolution of Western Ethiopia: igneous geochemistry, isotope systematics and U–Pb ages

T. GRENNE*†, R. B. PEDERSEN‡, T. BJERKGÅRD*, A. BRAATHEN*, M. G. SELASSIE§ & T. WORKU§

*Geological Survey of Norway, N-7491 Trondheim, Norway
‡Department of Geology, University of Bergen, N-5007 Bergen, Norway
§Geological Survey of Ethiopia, PO Box 2302, Addis Ababa, Ethiopia

(*Received* 15 July 2002; *accepted* 10 April 2003)

Abstract – New geochemical, isotopic and age data from igneous rocks complement earlier models of a long-lived and complex accretionary history for East African Orogen lithologies north of the Blue Nile in western Ethiopia, but throw doubt on the paradigm that ultramafic complexes of the region represent ophiolites and suture zones. Early magmatism is represented by a metavolcanic sequence dominated by pyroclastic deposits of predominantly basaltic andesite composition, which give a Rb–Sr whole-rock errorchron of 873 ± 82 Ma. Steep REE patterns and strong enrichments of highly incompatible trace elements are similar to Andean-type, high-K to medium-K calc-alkaline rocks; ε_{Nd} values between 4.0 and 6.8 reflect a young, thin continental edge. Interlayered basaltic flows are transitional to MORB and compare with mafic rocks formed in extensional, back-arc or inter-arc regimes. The data point to the significance of continental margin magmatism already at the earliest stages of plate convergence, in contrast with previous models for the East African Orogen. The metavolcanites overlap compositionally with the Kilaj intrusive complex dated at 866 ± 20 Ma (U–Pb zircon) and a related suite of dykes that intrude thick carbonate-psammite sequences of supposedly pre-arc, continental shelf origin. Ultramafic complexes are akin to the Kilaj intrusion and the sediment-hosted dykes, and probably represent solitary intrusions formed in response to arc extension. Synkinematic composite plutons give crystallization ages of 699 ± 2 Ma (Duksi, U–Pb zircon) and 651 ± 5 Ma (Dogi, U–Pb titanite) and testify to a prolonged period of major (D_1) contractional deformation during continental collision and closure of the 'Mozambique Ocean'. The plutons are characterized by moderately peraluminous granodiorites and granites with ε_{Nd} values of 1.0–2.0. They were coeval with shoshonitic, latitic, trachytic and rare trachybasaltic intrusions with very strong enrichments of highly incompatible trace elements and ε_{Nd} of 0.4–8.0. The mafic end-member is ascribed to partial melting of enriched sub-continental mantle that carried a subduction component inherited from pre-collision subduction. Contemporaneous granodiorite and granite formation was related to crustal underplating of the mafic magmas and consequent melting of lower crustal material derived from the previously accreted, juvenile arc terranes of the East African Orogen.

Keywords: Neoproterozoic, Ethiopia, geochronology, lithogeochemistry, isotope ratios.

1. Introduction

The East African Orogen provides a complex record of intra-oceanic and continental margin magmatic and tectonothermal events and is one of several major orogenic belts formed during the Neoproterozoic 'Pan-African' assembly of Gondwana (Stern, 1994). East African Orogen lithologies north of the Blue Nile in western Ethiopia comprise a range of supracrustal and plutonic rocks representative of much of the orogen's development. Precambrian exposures in this area occupy a position of particular interest, being located between the juvenile Neoproterozoic crust of the Arabian–Nubian Shield in the northern part of the East African Orogen, and the older, predominantly gneissic Mozambique Belt in the south. Nevertheless, only limited work has been published from this part of the orogen over the last 30 years (see bibliography by Demessie, 1996), partly as a consequence of social and political problems and the inaccessibility of much of the area. In particular, there is a lack of geochronological, isotopic and chemical data that can relate the Western Ethiopian Shield to the Arabian–Nubian Shield, the Mozambique Belt or the Saharan metacraton.

An account of the geology of the Wembera–Kilaj transect was published by Braathen *et al.* (2001) and covers a central part of the currently investigated area (Fig. 1). On the basis of lithostratigraphy, structural geology and limited geochemical data, they proposed an original arc and back-arc setting which experienced later continental collision and tectonic shortening. This model is in conflict with previous interpretations

† Author for correspondence: tor.grenne@ngu.no

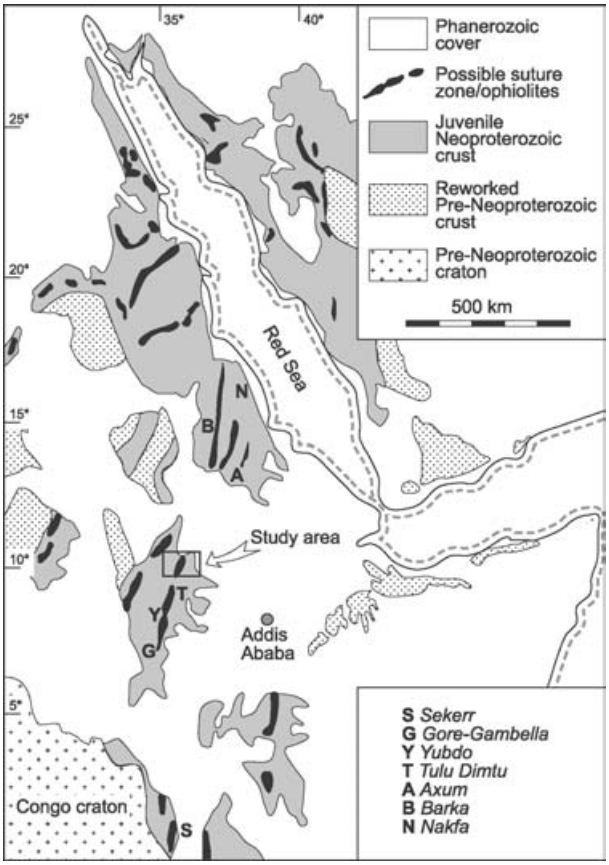

Figure 1. Generalized map of the Arabian–Nubian Shield, showing regional geological elements and locations as discussed in the text. Modified from Stern & Abdelsalam (1998) and Worku & Schandelmeier (1996).

of the region invoking the existence of a major suture zone separating exotic terranes. The present contribution presents new data with the emphasis on trace element and isotope geochemistry coupled with age determinations, with the aim to (1) identify the palaeotectonic setting of metavolcanic units and possible subvolcanic intrusions, (2) test the idea that mafic–ultramafic bodies represent layered intrusions rather than ophiolite fragments, (3) provide a model for the emplacement of synkinematic intrusive complexes, and (4) present a temporal framework for tectono-magmatic events and their relationship to major metasedimentary successions in this part of the East African Orogen.

2. Regional framework

Eastern Africa and the Arabian–Nubian Shield are generally thought to represent fragments of the ancient supercontinent Gondwana (Stern, 1994; Meert, 2003). The assembly of the eastern part of this supercontinent resulted from a complex series of events spanning a time interval from approximately 750 to 530 Ma. Of the two main orogenic periods that can be identified, the older one is usually referred to as the East African Orogen in accordance with the terminology of Stern (1994). The East African Orogen is thought of as a zone of continent–continent collision at the scale of the modern Alpine–Himalayan orogen.

In its northern part, the Arabian–Nubian Shield region comprises a collage of juvenile arc terranes and associated ophiolite fragments formed in the Neoproterozoic 'Mozambique Ocean' (Stern, 1994; Meert, 2003; and references therein). Stern (1994) argued that the opening of this ocean took place at *c*. 900 Ma followed by collision and amalgamation of the various terranes by *c*. 650 Ma. Based on a more recent compilation of age and geochemical data, Stern & Abdelsalam (1998) concluded that most of the juvenile Arabian–Nubian Shield crust formed in intra-oceanic convergent margin settings. Amalgamation of these terranes may have begun as early as 800 Ma and continued to *c*. 620 Ma.

Blasband *et al.* (2000) suggested on the basis of a compilation of available data on geochronology and palaeotectonic setting, mainly from the Arabia–Egypt–Sudan parts of the Arabian–Nubian Shield, that ophiolite development commenced at *c*. 900 Ma and persisted until *c*. 740 Ma. Arc development was largely overlapping with the ophiolites, possibly with a progressive change from early (900–850 Ma) primitive tholeiitic to late (825–730 Ma) evolved, calc-alkaline magmatism. Arc accretion took place at *c*. 750–650 Ma and strike-slip movements related to the later stages of this phase started at *c*. 670 Ma. A recent synopsis of events related to the assembly of Eastern Gondwana by Meert (2003) indicates that the East African Orogen formed through a series of arc collisions in the Arabian–Nubian Shield region from *c*. 750 Ma. This was followed at 640 ± 20 Ma by oblique continent–continent collision of east African crustal elements with a collage of continental blocks including parts of Madagascar, Sri Lanka, Seychelles, India and East Antarctica. Subsequent extensional collapse and post-orogenic magmatism started at about 600 Ma.

The limited data available on geochronology and magmatic petrology in the Precambrian of Western Ethiopia is mostly in accordance with the models from other parts of the Arabian–Nubian Shield. The broadly N–S-striking units of the region have been divided into Neoproterozoic and Palaeoproterozoic or, possibly, Archaean domains. Single zircon Pb–Pb ages from gneisses in eastern and southern Ethiopia (Teklay *et al.* 1998) indicate Palaeo- to Mesoproterozoic elements locally, but the majority of dated rocks are between 850 and 550 Ma and it is not clear whether the older ages represent the protoliths or inherited zircon xenocrysts. In western Ethiopia the exact ages of the supposedly older domains, as well as the nature of contacts between the domains, are unknown. Along the regional strike from the presently studied area, U–Pb zircon dating in the Gore-Gambella district south of the Blue Nile region (Fig. 1) indicates an age range of 837–769 Ma (within error) for pre- to supposedly synkinematic

https://doi.org/10.1017/S001675680300801X Published online by Cambridge University Press

plutons of calc-alkaline affinity; two post-kinematic granitic intrusions of shoshonitic affinity were emplaced between 582 and 525 Ma (Ayalew *et al.* 1990; Ayalew & Peccerillo, 1998). Near Axum to the north (Fig. 1), geochronological work by Tadesse, Hoshino & Sawada (1999) and Tadesse *et al.* (2000) yielded a zircon age of 757 ± 30 Ma for a calc-alkaline granitoid that intruded older metavolcanic units of tholeiitic arc affinity.

Further north, the Nakfa terrane in Eritrea (Fig. 1) has yielded zircon ages of *c*. 811 Ma for a supposedly syntectonic granitoid and about 850 Ma for felsic volcanic rocks (Teklay, 1997). Similarly, Kröner *et al.* (1991) reported a zircon age of *c*. 827 Ma for granite emplaced into *c*. 850 Ma peralkaline metarhyolites and associated marginal basin type metabasalts in the southeastern part of the Sudanese Red Sea Hills. Trondhjemite and tonalite that intruded older calc-alkaline metavolcanic sequences of oceanic arc affinity gave ages around 850–870 Ma. Recently, work in the Nakfa region by Teklay, Kröner & Mezger (2002) has given a U–Pb zircon age of 854 ± 3 Ma for a metarhyolite that belongs to a calc-alkaline volcanic sequence of oceanic arc affinity.

An important aspect of the understanding of the Arabian–Nubian Shield is the interpretation of N–S-oriented, curvilinear, regional shear zones hosting mafic and ultramafic rocks of supposedly ophiolitic character. Although complete ophiolite sequences are unknown in Western Ethiopia, these rocks have generally been interpreted to be remnants of the 'Mozambique Ocean' or, alternatively, back-arc basins within this major ocean (see review by Blasband *et al.* 2000). In these models, the mafic and ultramafic rocks are remnants of oceanic crust preserved along sutures that separate different arc terranes, and which were accreted during the assembly of pre-Gondwana crustal elements and sequences from the intervening ocean (e.g. Kröner, 1984; Stern, 1994). An alternative model was favoured by Braathen *et al.* (2001) for the Baruda–Tulu Dimtu zone. This stretches through Western Ethiopia and apparently adjoins with the Barka zone in Eritrea, and is one of the major structures of this type within the Arabian–Nubian Shield. According to this study, the mafic and ultramafic bodies along the shear zone, as well as isolated bodies on both sides, were originally emplaced as solitary magma chambers with mafic and ultramafic cumulates, as a consequence of limited dilation within a back-arc basin without the development of true oceanic crust. The extensive shearing associated with these plutons was probably controlled by competence contrasts to the marble-dominated country rocks.

3. Geological setting of the Blue Nile–Beles area

The investigated area covers a variety of metavolcanic and metasedimentary sequences, mafic–ultramafic mega-lenses and minor intrusions, as well as composite mafic to felsic plutonic complexes of batholithic dimensions (Fig. 2) that are very well exposed along numerous rivers in the mountainous terrain. All these units were affected by a regional compressional deformation phase designated D_1 by Braathen *et al.* (2001). This deformation was heterogeneous and has left many domains where the various rock types show well-preserved primary structures and textures. In particular, internal parts of large, rigid intrusions have escaped deformation.

The overall N–S-striking and steeply E-dipping D_1 foliation is most pronounced and penetrative in supracrustal rocks, but is also well developed in marginal parts of the intrusions. High-strain zones are found along lithological contacts, and also make up the bulk of the kilometre-wide Baruda shear belt. Highly D_1-strained rocks show a stretching lineation that commonly plunges to the east. Shear-sense indicators demonstrate top-to-the-W transport with a minor dextral component, possibly related to the development of W-verging thrust zones that were rotated to steep attitudes during progressive shortening, as discussed in Braathen *et al.* (2001). Greenschist- to lower amphibolite-facies metamorphism accompanied the D_1 deformation.

The several-kilometre-thick Baruda shear belt (Fig. 2) is a very prominent expression of the D_1 tectono-thermal event, comprising mylonitic supracrustal rocks and mafic–ultramafic mega-lenses. This belt constitutes a portion of the regional Sekerr–Yubdo–Barka suture zone of Berhe (1990), referred to as the Barka–Tulu Dimtu suture by Abdelsalam & Stern (1996) (Fig. 1). It is obvious that significant displacement took place along the Baruda shear belt, probably related to thrusting (Braathen *et al.* 2001). Nevertheless, on a larger scale, regional lithostratigraphic correlations can be made across the shear belt, indicating that a major terrane boundary or suture, as inferred by some authors, is unlikely (cf. discussion in Braathen *et al.* 2001).

Several shear zones of regional extent (D_2 of Braathen *et al.* 2001) are superimposed on the D_1 structures, and partly truncate the Baruda shear belt (Fig. 2). They are recorded as 200–300 m wide, N–S- to NNW–SSE-striking, subvertical shear zones, consisting of phyllonites that show a nearly horizontal stretching lineation. Cross-cutting relationships and shear-sense indicators can be related to sinistral transcurrent movements.

3.a. Mora metasediments

Metasedimentary units on both sides of the Baruda–Tulu Dimtu shear belt are characterized by an abundance of calcite marbles with occasional dolomitic varieties. It is the principal lithology of a more than 50 km wide unit east of the Baruda shear belt

https://doi.org/10.1017/S001675680300801X Published online by Cambridge University Press

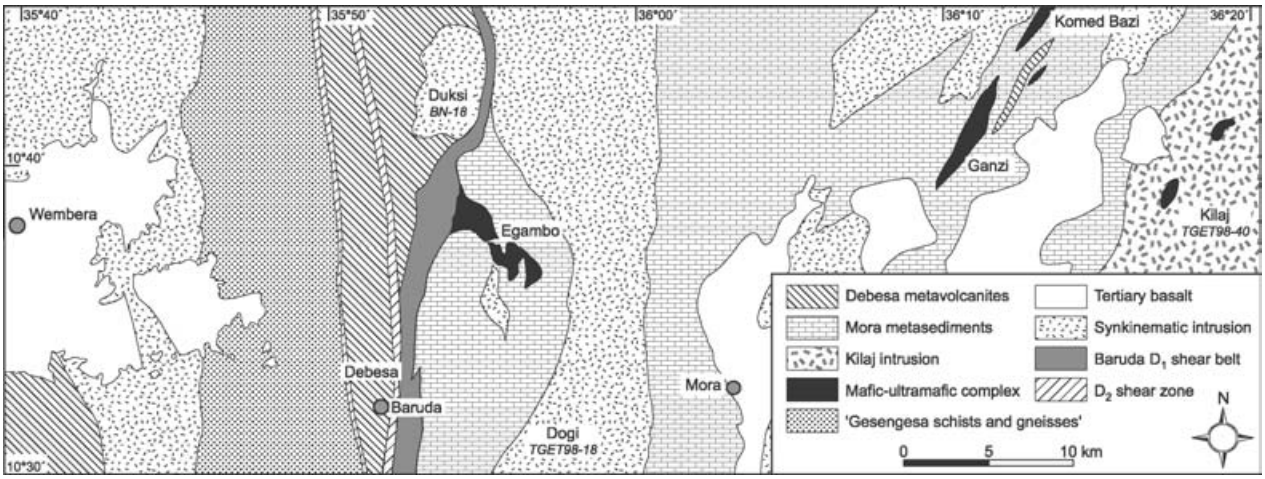

Figure 2. Geological east–west section of the Kilaj–Wembera area, Western Ethiopia, showing major lithological units and sample locations for U–Pb geochronology.

(Fig. 2), informally referred to as the Mora metasediments (Braathen *et al.* 2001). Homogeneous and very pure marbles with only a vague sedimentary layering are common and cover large areas. True thickness of the carbonate deposits is unknown due to folding, but it certainly was in the order of hundreds of metres or more. Laminated marble with thin interlayers or thicker, conformable units of quartzite, graphite-bearing marble or graphitic metapelite is found locally.

Feldspathic and locally arkosic metasandstone with local conglomerates are predominant in parts of the sequence and make up successions with an apparent thickness of several hundred metres; highly calcareous psammite and semipelite are subordinate lithologies. The arkosic and conglomeratic varieties are composed mainly of coarse-grained detritus of granitic composition. Much of the succession is reminiscent of alluvial fan deposits, but sedimentary facies interpretations are hampered by deformation and metamorphic recrystallization. Marbles and clastic units appear to have conformable contacts with no evidence of a major stratigraphic or structural break.

Identical lithologies are also quite abundant west of the shear belt, although they are generally more deformed and intercalated with tectonic slivers of metavolcanic rocks in a composite unit previously referred to as the 'Gesengesa schists and gneisses' (Tefera, 1991; Braathen *et al.* 2001) (Fig. 2). Much further west, thick sequences similar to the Mora metasediments occur in several places between the Baruda shear belt and the Sudanese border (Tefera, 1991).

3.b. Debesa metavolcanites

The Debesa metavolcanites form a several-kilometre-thick unit situated primarily west of the Baruda shear belt; similar units occur more locally to the east (Fig. 2). Contacts to the Mora metasediments are purely tectonic, and there is no unambiguous field evidence for the stratigraphic relationships between the Mora and Debesa units.

Two major volcanic elements can be distinguished in the Debesa unit (Braathen & Grenne, 1997; Braathen *et al.* 2001). Volumetrically, the most important is a series of intermediate rocks with subordinate felsic varieties. These metavolcanites are characterized by their commonly porphyritic nature, with 1–2 cm euhedral phenocrysts of plagioclase. Pyroclastic products are widespread and include lapilli tuff, lithic tuff, agglomerate and pyroclastic breccia; compositionally similar lava flows are massive or blocky.

Interlayered with the porphyritic andesites and associated metavolcanites, generally aphyric metabasalts constitute several separate units that range in thickness from *c*. 10–100 m. The majority are massive flows. Xenoliths of porphyritic andesite have been observed locally and attest to the close stratigraphic relations between the two types of Debesa metavolcanites. In places, highly amygdaloidal and pillowed varieties indicate a shallow subaqueous volcanic environment.

Metasedimentary units, a few tens of metres thick, comprise a significant part of the sequence and separate lava flows and pyroclastites at various stratigraphic levels (Braathen & Grenne, 1997). They are mostly mixed pyroclastic–epiclastic deposits of tuffaceous sandstone and siltstone with interlayers of graphitic schist, together with thin conglomerates composed of volcanic-derived debris. Sedimentary carbonate-andesite breccia is found locally.

3.c. Intrusive rocks

3.c.1. Mafic–utramafic plutonic complexes and dykes

The 'Egambo ultramafites' constitute a series of tectonically displaced rocks of both ultramafic and

https://doi.org/10.1017/S001675680300801X Published online by Cambridge University Press

mafic composition that form large bodies along the Baruda shear belt. They are enclosed in marble or locally border on the Debesa metavolcanites, however, their contacts are always highly sheared and primary contact relations have not been observed. The array of plutonic bodies extends into similar rocks north and south of the mapped area (Tefera, 1991, 1997) and is a direct extension of the Tulu Dimtu–Yubdo zone. A belt of similar mafic–ultramafic complexes is located in the Ganzi and Komed Bazi areas and a third belt occurs still further east (Fig. 2).

The plutonic complexes comprise serpentinite and talc ± tremolite ± chlorite rocks that grade into various metagabbros. Ultramafic rocks locally display relics of an igneous lamination. Most ultramafites are pervasively altered and their primary mineralogy is unknown. Normative compositions indicate that their precursors may have included dunite, harzburgite, wehrlite and clinopyroxenite, but the validity of norm calculations in such highly altered rocks is questionable. Little altered varieties occur locally and include nearly monomineralic hornblendite adcumulates with only accessory clinopyroxene. Layered metagabbros are found in several places and show a diffuse banding or a well defined, centimetre-scale, rhythmic layering, in some cases also including thin anorthositic bands (Bjerkgård, 1997). Hornblende is an important primary phase and may constitute 50 % or more also in the least metamorphosed gabbroic rocks, which include orthocumulates with clinopyroxene and plagioclase (An_{65-75}) as additional major phases.

Pre-tectonic metadolerites are abundant within the gabbroic rocks and also occur locally in ultramafic parts of the complexes. Some dykes exhibit highly irregular and unchilled contacts that branch into the hosting gabbro, and must have formed before the gabbro was completely crystallized.

Variably deformed, but clearly pre-tectonic, metadolerites are also commonly encountered in the Mora marbles, where they range from less than a metre up to 10 m or more across (Grenne *et al.* 1998). These dykes (here referred to as the 'Mora dykes') are aphyric and have well-defined chilled margins. In areas of moderate deformation they evidently form swarms with a dyke density of up to 10 %, the density being apparently greatest in the surroundings of the mafic–ultramafic bodies of the Egambo and Ganzi–Komed Bazi areas (Fig. 2).

3.c.2. The Kilaj intrusive complex

The Kilaj intrusive complex (Fig. 2) comprises a suite of plutonic rocks ranging from metagabbro to metadiorite and quartz diorite, the intermediate members being most common. Serpentinized ultramafic bodies are found in parts of the complex, but their contacts to the surrounding intrusive rocks have not been observed. Much of the complex is only moderately altered, mafic to intermediate varieties containing fresh plagioclase and primary hornblende with less clinopyroxene and subordinate biotite. Porphyritic metadiorite characterized by large plagioclase phenocrysts is ubiquitous. Biotite is abundant in the quartz dioritic varieties of the complex, and is locally accompanied by accessory garnet that is strongly resorbed. Extensive hornblende pegmatites are intimately associated with fine-grained gabbroic to dioritic rocks.

A vague mineral fabric reminiscent of igneous lamination is observed locally in mafic parts of the complex. In places, regular mafic dykes with unchilled margins cut the lamination at right angles. More characteristic, however, are complex mutual intrusive relationships between the different rock types, for example, between various mafic and felsic types or between fine-grained mafic and coarser porphyritic varieties (Grenne *et al.* 1998).

3.c.3. Synkinematic plutons

Synkinematic intrusive complexes that intrude all types of supracrustal rocks are represented by the Dogi and Duksi complexes (Fig. 2). Dogi is a large, N–S-trending batholith located in the central-eastern part of the investigated area, while Duksi is a smaller complex located west of the Baruda shear belt (Braathen *et al.* 2001). Both are composite intrusions dominated by grey to pinkish grey biotite-bearing granodiorites and granites; muscovite and garnet are additional minor phases at Duksi. In both complexes, the granitoids show mutual intrusive relationships and mingling with a suite of essentially intermediate intrusives. These range from fine-grained, biotite–muscovite-rich dioritoids (Dogi) to medium-grained, biotite–muscovite-bearing rocks with the modal compositions of quartz monzonite (Duksi); both have plagioclase compositions that cluster at An_{20-30}.

The Dogi and Duksi complexes are only moderately affected by metamorphic alteration. Interior parts of the intrusions show in general little or no sign of deformation, whereas their contact zones were highly strained during D_1 with an outward decreasing density of sheared and boudinaged granitic apophyses. Less deformed parts of the Dogi contact zone are characterized by marble rafts and an extensive network of dykes in the surrounding lithologies. Comparable relationships are seen along the mainly metavolcanite-hosted Duksi intrusion. In both cases, some of the granitoid dykes truncate ductile shear structures and are variably folded by the same D_1 structures. These folded and sheared dykes were subsequently intersected by similar, but undeformed, dykes (Grenne *et al.* 1998). Similar evidence of synkinematic intrusion can be seen more locally in central parts of the plutonic complexes.

https://doi.org/10.1017/S001675680300801X Published online by Cambridge University Press

4. U–Pb geochronology

Zircon and titanite were separated from the rock samples using standard crushing and mineral separation procedures. Zircon concentrates were divided into bulk fractions based on grain size and magnetic susceptibility, and the fractions were selected for analyses by hand-picking under microscope. Most of the zircon fractions were abraded to minimize surface correlated Pb-loss. After washing in distilled H_2O, hot 6N HNO_3, and distilled acetone, the zircon fractions were weighed into Teflon bombs with a mixed $^{205}Pb/^{235}U$ spike and HF and HNO_3. The titanite fractions were dissolved in Savillex vials with HF and HNO_3 on the hot plate over two days. Pb and U were separated by standard chromatographic techniques in miniature Teflon columns. Pb and U were loaded together on single Re-filaments with H_3PO_4 and silica gel. The isotopic analyses were carried out on a Finnigan MAT262 at the Department of Geology, University of Bergen. Analytical uncertainties on the Pb/U and the $^{207}Pb/^{206}Pb$ ratios were calculated using the procedure given by Ludwig (1980). The results of the analyses are given in Table 1.

Kilaj intrusive complex (sample TGET98-40). The sample is a medium-grained quartz diorite from the central part of the Kilaj complex. The quartz diorite is a few tens of metres across, and shows transitional contacts and mingling relationships to metadiorite and metagabbro of the main complex. Highly resorbed garnet is an accessory phase. Three fractions of small, euhedral zircon prisms were analysed. The fractions plot from 11 % to 5 % discordant (Fig. 3a). The best fit line through the three data points yields an imprecise intercept age of 866 ± 20 Ma.

Duksi synkinematic intrusion (BN-18). The analysed rock is a medium-grained, pinkish grey biotite-bearing granodiorite with minor amounts of garnet, sampled *c*. 400 m from the contact zone of the Duksi complex. Five fractions of euhedral zircon prisms were analysed. The fractions plot from 0.25 % to 5 % discordant. The $^{207}Pb/^{206}Pb$ age of four of the fractions range from 698.4 to 700.4 with an average of 698.9 ± 1.7 Ma. A fifth fraction gave a slightly younger age of 694.9 Ma. The best fit line through the data points yields an upper intercept of 698.6 ± 2.5 Ma (Fig. 3b). We consider the 699 ± 2 Ma to be the age of this granitoid.

Dogi synkinematic intrusion (TGET98-18). The fine-grained, greyish biotite-bearing granodiorite is from the western contact zone of the Dogi complex, where felsic and associated intermediate intrusions form a network of dykes in the wall-rock marbles. Two fractions of transparent, brown titanites were hand-picked and analysed. Both fractions yielded $^{238}U/^{206}Pb$ and $^{235}U/^{207}Pb$ that are concordant within errors (Fig. 3c). A high common lead content resulted in low $^{206}Pb/^{204}Pb$ which makes the $^{207}Pb/^{206}Pb$ age imprecise. With high common lead contents the $^{238}U/^{206}Pb$

Table 1. U–Pb isotopic age data for rocks from the investigated part of the Arabian-Nubian Shield in Western Ethiopia

Fractions			Concentrations		Measured		Atomic ratios								Age (Ma)					
No.	Properties	Wt. (mg)	U (ppm)	Pb rad (ppm)	Pb t.c. (pg)	$^{206}Pb/^{204}Pb$	$^{208}Pb/^{206}Pb$	$^{206}Pb/^{238}U$	±	$^{207}Pb/^{235}U$	±	R	$^{207}Pb/^{206}Pb$	±	$^{206}Pb/^{238}U$	±	$^{207}Pb/^{235}U$	±	$^{207}Pb/^{206}Pb$	±
98-40-a	zircon, 1 M, abr	0.028	394.0	51.4	60	1260	0.1457	0.12240	48	1.1284	53	0.87	0.06687	15	744.3	2.8	767.0	2.5	833.7	4.8
98-40-b	zircon, 1 M, abr	0.010	363.0	59.0	89	333	0.2249	0.13472	193	1.2544	194	0.93	0.06753	38	814.7	11.0	825.4	8.8	854.2	11.8
98-40-c	zircon, 1 M, abr	0.010	410.1	60.1	67	461	0.1844	0.12841	42	1.1895	59	0.71	0.06718	23	778.8	2.4	795.7	2.7	843.5	7.25
BN-18-a	zircon 7 M, abr	0.030	197.5	24.8	53	711	0.1772	0.11354	25	0.9817	34	0.73	0.06271	15	693.3	1.5	694.5	1.7	698.4	5.12
BN-18-b	zircon 7 M	0.063	302.0	34.0	75	1567	0.1310	0.10780	31	0.9318	30	0.92	0.06269	8	659.9	1.8	668.6	1.6	697.9	2.58
BN-18-c	zircon 7 M, abr	0.060	290.9	34.3	72	1540	0.1246	0.11346	27	0.9817	28	0.88	0.06275	9	692.8	1.6	694.5	1.5	699.9	2.91
BN-18-d	zircon 7 M, abr	0.050	188.6	22.9	60	998	0.1394	0.11447	37	0.9907	45	0.74	0.06277	19	698.7	2.1	699.1	2.3	700.4	6.46
BN-18-e	zircon 7 M, abr	0.114	300.1	34.8	89	2493	0.1257	0.11217	30	0.9683	34	0.89	0.06261	11	685.3	1.7	687.6	1.8	694.9	3.59
98-18-a	titanite, brown frag	0.250	80.6	14.0	1467	106	0.3964	0.10635	30	0.8888	140	0.24	0.06061	93	651.5	1.8	645.7	7.6	625.6	33.4
98-18-b	titanite, brown frag	0.314	98.8	14.0	1219	181	0.2578	0.10626	29	0.8959	83	0.35	0.06114	52	651.0	1.7	649.5	4.4	644.3	18.6

M = magnetic fractions; R = correlation coefficient of errors in isotopic ratios; abr = abraded; frag = fragments; t.c. = total common; rad = radiogenic. The measured $^{206}Pb/^{204}Pb$ ratios are corrected for fractionation and common lead in spike. Atomic ratios are corrected for fractionation and spike, lab Pb blank of 5 pg (30 pg – titanite) and initial common Pb at the time of the sample, calculated using the model of Stacey & Kramers (1975) and 2 pg U blank. Uncertainties on the isotopic ratios are calculated with the error propagation procedure of Ludwig (1980), and are reported at the 2σ confidence level.

https://doi.org/10.1017/S001675680300801X Published online by Cambridge University Press

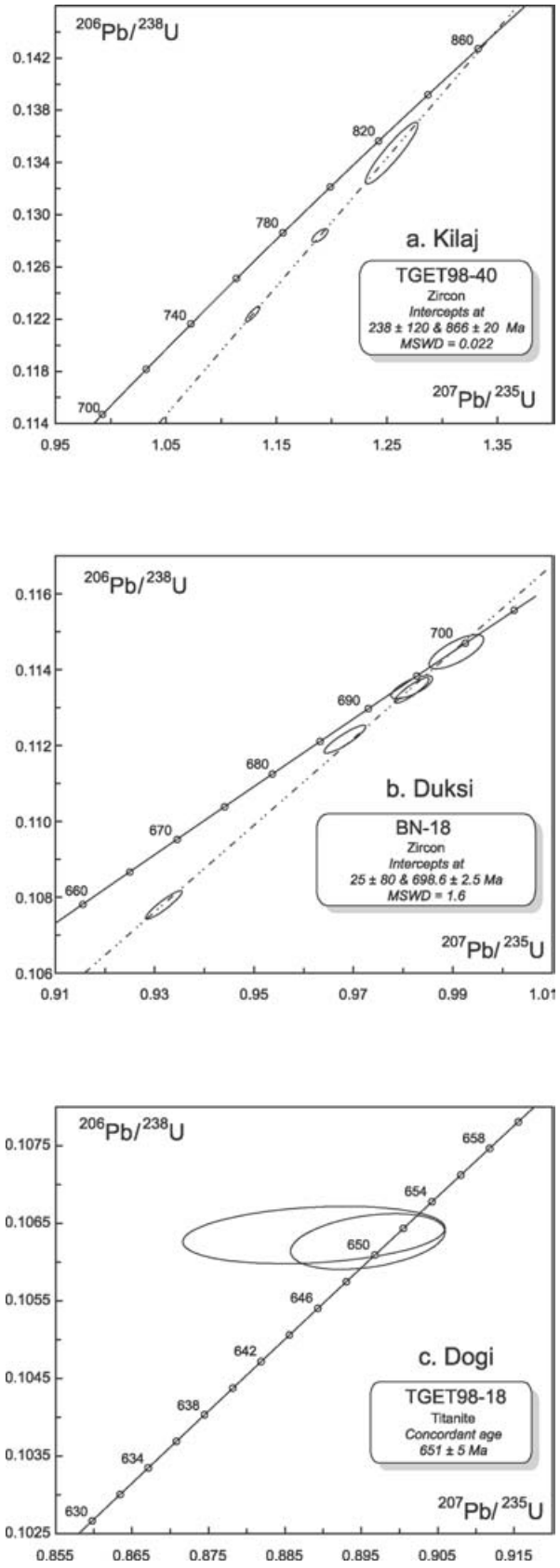

Figure 3. U–Pb concordia diagram showing zircon and titanite data from plutonic rocks of the East African Orogen in Western Ethiopia. (a) Kilaj intrusive complex; (b) Duksi synkinematic pluton; (c) Dogi synkinematic pluton. See text for description of rock types.

ages are the most precise geochronometer. The $^{238}U/^{206}Pb$ ages of the two fractions are 651.0 and 651.5 Ma, and we consider 651 ± 5 Ma to be the age of crystallization of this granitoid.

5. Geochemistry

5.a. Analytical procedures

X-ray fluorescence (XRF) analyses were carried out by the Geological Survey of Norway, using standard XRF techniques on fused glass beads prepared by 1 : 7 dilution with lithiumtetraborate (major elements), and on pressed powder pellets (trace elements). The samples were analysed on a Philips PW 1480 sequential X-ray spectrometer equipped with a Sc/W-anode X-ray tube, using common international standards for calibration.

Additional trace elements, including the rare earths (REE) were analysed by a SCIEX ICP-MS instrument at the Centre for Earth Resources Research, Memorial University of Newfoundland. Samples of mafic rocks were analysed after a multi-acid digestion, using the method of standard addition to correct for matrix effects. Samples of intermediate and felsic rocks were digested using sodium peroxide sinters to ensure dissolution of all minerals including zircons. Full details of the ICP-MS procedures are given by Jenner *et al.* (1990) and Longerich *et al.* (1990). A representative set of analyses from the different units is included in Table 2 and Figures 4 to 7.

5.b. Pre-D_1 igneous rocks

The Debesa metavolcanites form a continuum of rocks with silica contents ranging from that of basalts and basaltic andesites, to subordinate andesites and dacites (Le Maitre *et al.* 1989). Metarhyolites are rare. Al_2O_3 contents of mafic and intermediate members cluster around 17.5 %. The basaltic andesites and more felsic metavolcanites define a clear calc-alkaline trend in a (Na_2O+K_2O)–FeO_{total}–MgO (AFM) diagram (not shown), whereas the basaltic rocks straddle the calc-alkaline/tholeiite boundary and indicate a poorly defined iron-enrichment trend.

The Kilaj complex shows a major element compositional span similar to that of the Debesa metavolcanites. Dykes in the Mora sedimentary sequence and gabbro-hosted dykes range from basaltic to minor basaltic andesite. The metamorphic ultramafites are chemically diverse and range from dunitic to normal gabbroic or basaltic compositions. Some varieties overlap with the compositions of the locally preserved primary hornblendites; however, the distinction of hornblende-bearing versus pyroxene- and plagioclase-bearing types is difficult on the basis of major elements in these completely recrystallized rocks.

https://doi.org/10.1017/S001675680300801X Published online by Cambridge University Press

Table 2. Major and trace element data for metavolcanic and intrusive rocks from the investigated part of the Arabian-Nubian Shield in Western Ethiopia

Unit	Debesa metavolcanites							Kilaj hornblende diorite complex						Dykes in Mora sedim. seq.		
Type	Basalts			Basaltic andesites – dacites										Metadolerites		
Sample	BW 01	BW 05	BW 10	BN 05	BN 06	BN 08	BW 16	TGET 98-38	TGET 98-39	TGET 98-41	TGET 98-42	TGET 98-43	TGET 98-44	MQ 01	MQ 03	MQ 14
Long.	35°50′46″	35°51′48″	35°51′40″	35°53′38″	35°53′38″	35°53′38″	35°51′25″	36°21′18″	36°21′21″	36°25′06″	36°25′02″	36°25′02″	36°24′55″	35°57′15″	35°57′13″	35°57′26″
Lat.	10°32′51″	10°32′07″	10°32′10″	10°40′28″	10°40′28″	10°40′28″	10°32′15″	10°36′07″	10°36′13″	10°35′36″	10°35′36″	10°35′36″	10°35′36″	10°34′40″	10°34′50″	10°33′51″
wt %																
SiO_2	50.22	46.90	50.41	53.53	61.05	55.38	53.83	47.09	57.37	69.14	55.98	54.40	49.07	48.92	53.20	46.58
TiO_2	1.07	0.93	1.19	0.85	0.80	0.82	1.12	1.17	0.73	0.39	0.66	0.79	0.73	0.96	1.15	1.24
Fe_2O_3	9.40	9.93	10.77	9.12	6.36	8.71	7.84	12.17	7.03	3.17	10.11	8.16	10.94	10.54	9.02	10.75
Al_2O_3	16.64	16.22	15.86	16.84	18.06	15.06	17.88	19.62	17.09	15.81	17.36	18.64	15.19	17.11	17.32	15.72
MnO	0.15	0.17	0.14	0.10	0.04	0.19	0.15	0.21	0.10	0.06	0.17	0.11	0.20	0.19	0.13	0.17
MgO	8.04	6.54	6.94	4.73	3.02	7.18	3.24	4.29	3.52	1.33	1.49	2.21	7.82	5.51	4.56	9.06
CaO	10.19	10.03	7.26	6.37	1.13	4.61	4.75	9.55	6.61	3.42	5.41	7.25	10.41	10.37	8.07	11.79
Na_2O	2.86	2.73	3.78	2.65	2.59	2.52	3.57	3.55	4.02	4.19	4.37	4.09	2.33	3.34	3.83	2.20
K_2O	0.18	0.05	0.32	2.57	3.48	2.78	2.93	0.40	1.45	2.23	1.36	0.93	0.73	0.50	1.07	0.26
P_2O_5	0.24	0.20	0.22	0.39	0.28	0.28	0.58	0.42	0.24	0.17	0.55	0.25	0.23	0.21	0.30	0.23
L.O.I.	0.70	6.97	2.95	2.55	2.50	1.86	4.69	0.89	0.76	0.64	0.55	3.11	1.31	1.58	1.01	0.75
Total	99.70	100.67	99.83	99.71	99.32	99.38	100.57	99.36	98.91	100.54	98.01	99.94	98.97	99.22	99.66	98.73
ppm																
Sc	36	32	35	28	26	35	19	26	15	<10	<10	<10	36	32	25	31
V	206	192	186	216	132	157	131	173	144	40	11	65	227	207	186	207
Cr	316	204	131	7	121	237	19	28	81	57	24	28	193	29	26	338
Ni	146	41	30	10	43	115	15	8	50	15	<5	7	52	16	12	99
Co	43	46	35	22	12	39	27	27	26	<10	15	16	42	36	27	46
Cu	96	79	38	32	11	< 5	6	24	58	16	28	29	33	8	21	25
Zn	68	81	89	83	155	86	134	96	71	46	115	93	95	88	97	86
Sr	*347*	*512*	*218*	199	90	212	320	*818*	804	344	566	772	*499*	*508*	550	*273*
Ba	*58*	*34*	*270*	*1948*	*2956*	*444*	*753*	*154*	*798*	*586*	*519*	*615*	*309*	*190*	*533*	*75*
Rb	*3.24*	*1.22*	*3.31*	109	91	55	63	*4.97*	25	58	18	14	*10.59*	*8.66*	23	*3.75*
Cs	*0.16*	*0.08*	*0.23*					*0.13*					*0.17*	*0.23*		*0.07*
La	*12.99*	*6.09*	*7.87*	*16.22*	*20.92*	*20.90*	*31.09*	*10.82*	*10.90*	*17.80*	*22.52*	*13.63*	*6.67*	*7.36*	*17.11*	*4.77*
Ce	*29.11*	*14.87*	*19.47*	*33.67*	*43.58*	*47.75*	*65.61*	*28.50*	*24.83*	*33.14*	*50.15*	*28.04*	*16.07*	*18.34*	*40.46*	*13.48*
Pr	*3.81*	*2.23*	*2.93*	*4.29*	*5.49*	*6.15*	*8.19*	*4.35*	*3.46*	*3.67*	*6.69*	*3.72*	*2.36*	*2.76*	*5.51*	*2.22*
Nd	*16.25*	*10.48*	*14.28*	*19.02*	*22.57*	*26.22*	*35.14*	*20.52*	*16.02*	*13.59*	*28.78*	*16.76*	*11.30*	*13.25*	*24.76*	*11.54*
Sm	*3.73*	*2.95*	*4.04*	*4.20*	*4.90*	*5.48*	*7.38*	*5.02*	*3.86*	*2.57*	*6.36*	*3.95*	*2.91*	*3.56*	*5.45*	*3.83*
Eu	*1.24*	*1.07*	*1.47*	*1.13*	*1.16*	*1.49*	*2.00*	*1.71*	*1.07*	*0.73*	*1.85*	*1.25*	*0.99*	*1.25*	*1.53*	*1.30*
Gd	*3.86*	*3.41*	*4.65*	*3.89*	*4.47*	*4.77*	*6.85*	*5.14*	*3.41*	*2.11*	*5.97*	*3.51*	*3.00*	*4.05*	*5.02*	*4.79*
Tb	*0.64*	*0.55*	*0.74*	*0.53*	*0.67*	*0.67*	*0.98*	*0.80*	*0.48*	*0.28*	*0.90*	*0.45*	*0.47*	*0.66*	*0.71*	*0.82*
Dy	*4.07*	*3.58*	*4.80*	*3.33*	*4.28*	*3.98*	*5.80*	*4.86*	*2.88*	*1.55*	*5.36*	*2.46*	*2.89*	*4.19*	*4.05*	*5.40*
Ho	*0.84*	*0.76*	*0.98*	*0.68*	*0.91*	*0.83*	*1.17*	*1.02*	*0.53*	*0.31*	*1.15*	*0.44*	*0.61*	*0.88*	*0.82*	*1.13*
Er	*2.39*	*2.15*	*2.79*	*1.86*	*2.68*	*2.35*	*3.25*	*2.98*	*1.60*	*0.85*	*3.44*	*1.12*	*1.75*	*2.54*	*2.28*	*3.25*
Tm	*0.34*	*0.33*	*0.40*	*0.28*	*0.41*	*0.35*	*0.45*	*0.44*	*0.20*	*0.13*	*0.51*	*0.15*	*0.25*	*0.39*	*0.31*	*0.49*
Yb	*2.21*	*1.88*	*2.48*	*1.78*	*2.68*	*2.19*	*2.94*	*2.84*	*1.21*	*0.80*	*3.48*	*0.96*	*1.68*	*2.30*	*2.09*	*3.02*
Lu	*0.25*	*0.22*	*0.29*	*0.27*	*0.40*	*0.32*	*0.42*	*0.35*	*0.19*	*0.12*	*0.56*	*0.14*	*0.20*	*0.27*	*0.29*	*0.41*
Y	*21.21*	*19.31*	*24.39*	*17.17*	*23.98*	*21.61*	*29.95*	*26.05*	*13.15*	*7.95*	*30.11*	*11.22*	*15.70*	*22.74*	*20.82*	*28.89*
Zr	91	60	81	99	130	138	178	186	111	135	176	87	46	73	162	81
Hf	*0.58*	*0.24*	*0.68*	*3.37*	*2.96*	*3.30*	*4.45*	*1.31*	*3.39*	*3.58*	*3.95*	*2.43*	*0.83*	*0.35*	*4.21*	*0.53*
Nb	*8.52*	*1.14*	*3.11*	*5.37*	*9.39*	*6.58*	*10.44*	*4.66*	*3.37*	*9.99*	*16.92*	*6.40*	*1.75*	*2.39*	*7.81*	*2.16*
Ta	*0.38*	*0.09*	*0.17*	*0.16*	*0.53*	*0.22*	*0.34*	*0.20*	*0.22*	*0.67*	*0.75*	*0.33*	*0.08*	*0.13*	*0.17*	*0.13*
Th	*1.04*	*0.49*	*0.50*	*3.48*	*5.84*	*2.70*	*4.38*	*0.19*	*2.30*	*4.85*	*0.86*	*2.66*	*0.31*	*0.48*	*1.75*	*0.21*
U	*0.30*	*0.42*	*0.15*					*0.18*					*0.11*	*0.27*		*0.28*
Pb	*1.90*	*2.83*	*2.18*	< 10	< 10	13	< 10	*2.45*	< 10	< 10	< 10	< 10	*4.81*	*2.23*	< 10	*1.46*

Table 2. (*Cont.*)

Unit	Mafic-ultramafic complexes							Duksi synkinematic intrusion					Dogi synkinematic intrusion			
Type	Metadolerites		IMG	Layered metagabbros		LMPX	LHBL	Quartz monzonites			Granitoids		Diorites		Granitoids	
Sample	TGET 98-63	TGET 98-65	TGET 98-01	BE 01	BE 03	TBET 16	TGET 98-66	BN 14	BN 17	BN 18	BN 13	BN 19	TGET 98-19	TGET 98-21	TGET 98-13	TGET 98-18
Long.	36°10′36″	36°10′35″	35°56′30″	35°52′46″	35°52′46″	35°55′05″	36°10′33″	35°53′56″	35°54′05″	34°54′04″	35°53′41″	35°53′56″	35°57′17″	35°56′03″	35°56′11″	35°57′11″
Lat.	10°40′45″	10°40′53″	10°36′00″	10°31′25″	10°31′25″	10°37′25″	10°41′00″	10°40′45″	10°41′00″	10°40′56″	10°40′45″	10°40′48″	10°31′23″	10°30′38″	10°30′53″	10°31′15″
wt%																
SiO_2	46.89	47.90	38.57	48.69	42.41	47.98	46.20	62.87	59.14	67.30	73.22	76.94	59.12	57.03	70.77	71.24
TiO_2	0.85	1.71	0.99	0.79	0.19	0.16	0.31	0.82	0.51	0.35	0.23	0.09	1.21	1.39	0.23	0.24
Fe_2O_3	12.09	11.69	10.05	11.67	7.28	6.03	13.66	5.15	4.53	2.16	2.32	0.74	5.69	6.53	1.54	1.66
Al_2O_3	14.75	16.80	13.20	14.40	16.61	2.23	10.81	16.23	18.07	15.74	14.86	14.21	16.93	17.11	14.33	15.04
MnO	0.18	0.26	0.19	0.18	0.15	0.10	0.22	0.08	0.08	0.04	0.05	0.01	0.07	0.10	0.02	0.02
MgO	7.76	4.94	5.55	8.87	12.22	22.74	14.88	2.20	1.66	1.05	0.92	0.11	1.98	2.19	0.51	0.53
CaO	9.94	7.74	13.96	10.33	17.96	15.71	9.61	4.29	3.07	1.77	2.31	0.75	4.30	3.57	1.88	2.13
Na_2O	3.01	2.73	2.67	3.11	< 0.10	< 0.10	2.24	3.97	5.09	4.85	3.32	5.41	4.74	4.80	3.78	3.99
K_2O	0.29	1.69	0.18	0.07	0.02	< 0.01	0.06	2.45	5.25	3.69	3.12	1.50	3.58	3.35	4.12	3.89
P_2O_5	0.55	0.60	0.30	0.12	0.09	0.07	0.15	0.31	0.40	0.14	0.07	0.02	0.54	0.66	0.07	0.07
L.O.I.	1.73	2.84	13.97	1.72	3.64	3.46	2.03	1.63	1.48	2.65	0.92	1.08	0.58	1.26	0.53	0.35
Total	98.02	98.90	99.62	99.93	100.65	98.53	100.16	100.00	99.28	99.74	101.34	100.87	98.75	97.97	97.77	99.18
ppm																
Sc	42	24	30	43	38	43	47	15	11	< 10	< 10	< 10	< 10	< 10	< 10	< 10
V	294	193	269	273	158	134	225	81	84	36	39	9	83	91	25	22
Cr	96	< 5	117	299	486	2249	635	22	7	31	7	35	5	< 5	19	27
Ni	38	15	44	84	188	615	206	16	13	17	7	6	12	6	6	6
Co	36	30	34	52	52	69	72	12	< 10	< 10	< 10	< 10	12	12	< 10	< 10
Cu	51	80	127	28	161	16	19	8	< 5	< 5	21	13	14	32	9	< 5
Zn	89	84	59	92	42	26	109	81	53	31	28	8	77	86	29	30
Sr	*705*	*443*	*353*	*400*	373	*35.5*	*127*	618	2533	1327	209	362	909	760	389	470
Ba	*68*	*705*	*30*	*20*	*25*	*4*	*9*	*1082*	*3119*	*2105*	*341*	*382*	*1737*	*1419*	*1506*	*1530*
Rb	*2.83*	*27.69*	*2.09*	*0.98*	< 5	*0.09*	*0.23*	55	47	53	132	34	78	60	92	98
Cs	*0.04*	*0.28*	*0.09*	*0.03*		< 0.005	< 0.007									
La	*17.91*	*23.12*	*5.60*	*1.88*	*0.37*	*1.09*	*2.44*	*41.97*	*74.22*	*35.80*	*5.59*	*3.73*	*57.89*	*64.27*	*32.00*	*27.95*
Ce	*44.73*	*54.18*	*12.43*	*5.99*	*1.12*	*3.89*	*9.42*	*79.02*	*147.25*	*67.44*	*11.55*	*7.43*	*111.24*	*121.51*	*52.52*	*46.50*
Pr	*6.28*	*7.14*	*1.79*	*1.08*	*0.21*	*0.70*	*1.79*	*8.90*	*17.35*	*7.53*	*1.38*	*0.88*	*12.27*	*13.33*	*5.18*	*4.63*
Nd	*28.82*	*30.02*	*8.82*	*5.91*	*1.21*	*3.65*	*9.99*	*31.70*	*64.95*	*27.50*	*5.60*	*3.40*	*44.66*	*47.54*	*16.68*	*15.27*
Sm	*6.62*	*6.35*	*2.44*	*1.97*	*0.48*	*0.98*	*2.91*	*5.37*	*9.82*	*4.32*	*1.22*	*0.74*	*7.07*	*7.69*	*2.41*	*2.13*
Eu	*1.73*	*1.92*	*0.87*	*0.77*	*0.24*	*0.30*	*0.89*	*1.40*	*2.95*	*1.15*	*0.35*	*0.20*	*1.88*	*2.04*	*0.56*	*0.51*
Gd	*5.54*	*5.95*	*3.00*	*2.55*	*0.82*	*0.98*	*2.64*	*4.00*	*5.94*	*2.90*	*1.15*	*0.58*	*5.23*	*5.68*	*1.34*	*1.15*
Tb	*0.74*	*0.88*	*0.46*	*0.44*	*0.14*	*0.13*	*0.34*	*0.51*	*0.66*	*0.34*	*0.16*	*0.08*	*0.66*	*0.74*	*0.13*	*0.11*
Dy	*3.94*	*5.30*	*3.02*	*3.00*	*1.00*	*0.80*	*1.90*	*2.78*	*3.25*	*1.75*	*0.96*	*0.50*	*3.51*	*4.12*	*0.61*	*0.48*
Ho	*0.70*	*1.04*	*0.61*	*0.63*	*0.23*	*0.15*	*0.34*	*0.52*	*0.59*	*0.33*	*0.20*	*0.11*	*0.66*	*0.79*	*0.11*	*0.09*
Er	*1.88*	*2.91*	*1.75*	*1.92*	*0.73*	*0.41*	*0.97*	*1.47*	*1.61*	*0.88*	*0.57*	*0.35*	*1.75*	*2.14*	*0.27*	*0.25*
Tm	*0.26*	*0.40*	*0.25*	*0.27*	*0.10*	*0.05*	*0.14*	*0.21*	*0.23*	*0.12*	*0.09*	*0.05*	*0.24*	*0.29*	*0.04*	*0.03*
Yb	*1.51*	*2.54*	*1.55*	*1.82*	*0.64*	*0.34*	*0.88*	*1.25*	*1.49*	*0.77*	*0.57*	*0.35*	*1.48*	*1.86*	*0.24*	*0.24*
Lu	*0.16*	*0.29*	*0.20*	*0.23*	*0.09*	*0.03*	*0.10*	*0.19*	*0.24*	*0.11*	*0.08*	*0.05*	*0.22*	*0.28*	*0.04*	*0.04*
Y	*18.48*	*27.68*	*16.43*	*16.40*	*5.55*	*4.00*	*8.82*	*13.90*	*16.14*	*9.17*	*5.89*	*3.56*	*17.04*	*20.35*	*2.76*	*2.40*
Zr	83	182	43	25	< 5	9	14	299	601	162	87	61	387	443	140	170
Hf	*0.88*	*2.12*	*0.35*	*0.77*	*0.20*	*0.28*	*0.38*	*6.25*	*11.93*	*3.80*	*2.86*	*1.52*	*8.23*	*9.64*	*3.75*	*3.67*
Nb	*3.85*	*10.34*	*2.51*	*1.35*	*0.17*	*0.08*	*0.17*	*18.94*	*9.36*	*5.94*	*3.22*	*3.53*	*31.70*	*31.54*	*5.78*	*3.33*
Ta	*0.21*	*0.50*	*0.14*	*0.06*	*0.00*	*0.01*	*0.02*	*0.52*	*0.19*	*0.38*	*0.16*	*0.22*	*0.68*	*1.63*	*0.34*	*0.09*
Th	*2.21*	*1.72*	*0.25*	*0.09*	*0.01*	*0.04*	*0.03*	*5.30*	*2.24*	*4.97*	*3.87*	*2.03*	*4.46*	*5.35*	*11.18*	*10.81*
U	*1.14*	*0.82*	*0.15*	< 0.004		< 0.015	*0.02*									
Pb	*3.05*	*3.46*	*2.49*	*2.07*	< 10	*0.06*	*0.37*	17	28	25	36	10	< 10	16	< 10	< 10

Trace element analysis by ICP-MS in italics, other data by XRF. Details on analytical procedures are given in the text. Abbreviations for rock types: IMG = isotropic metagabbro, LMPX = layered metapyroxenite, LHBL = layered hornblendite

Mid-ocean ridge basalt (MORB)-normalized multi-element diagrams (Fig. 4a) show that the Debesa basaltic andesites, which make up the bulk of the metavolcanic sequence, are strongly enriched in the most incompatible trace elements. Among the immobile high-field-strength elements (HFSE), Th shows the strongest enrichment, with contents of 22–36 times that of normal mid-ocean ridge basalt. The highly incompatible large ion lithophile elements (LILE; Cs, Rb, Ba, K) generally conform to the Th enrichment pattern, even though they show a wider scatter that is probably due to the mobility of the LILE during sea-floor alteration and metamorphism. Less incompatible HFSE like the heavy rare earths (HREE) are comparable to or slightly lower than MORB. With consistently large negative anomalies for Nb–Ta and Ti and moderate Zr–Hf anomalies, the basaltic andesite patterns show similarities to modern calc-alkaline rocks (Fig. 4a). Moreover, their strong incompatible-element enrichment and steep REE patterns (La_N/Yb_N ratios 6.5–9) are comparable to high-K to medium-K calc-alkaline volcanic rocks found at active continental margins rather than to calc-alkaline rocks of oceanic island arcs (e.g. Pearce *et al.* 1995*b*).

Andesitic to dacitic metavolcanites from the Debesa sequence have largely similar trace element and REE patterns (Fig. 4a), suggesting they may belong to the same differentiation series as the basaltic andesites. Increasing negative anomalies for P, Ti and Eu in the more felsic varieties probably reflect crystallization of apatite, Fe–Ti oxides and plagioclase.

The mafic lavas intercalated in the Debesa sequence share many of the geochemical characteristics of the basaltic andesites (Fig. 4b). However, significant differences are evident in the less pronounced incompatible-element enrichments (Th enrichment = 4–8X MORB; La_N/Yb_N ratios = 2–4) which are more like those of low- to medium-K volcanic rocks, and the smaller and less consistent negative anomalies for Nb–Ta and Ti in the MORB-normalized patterns for the metabasalts. Mg-numbers are relatively low ($Mg/(Mg + Fe) \leq 0.42$). Coupled with low Ni values (Table 2), this indicates that the erupting basaltic magmas were not primary mantle derived melts but were significantly modified by fractional crystallization (e.g. Wilson, 1989). Large variations in highly-incompatible trace element ratios, such as Th/Ta and La/Nb, indicate the existence of differences in the source region since fractional crystallization is practically unable to modify these ratios; this applies also to the differences between the basaltic and the andesitic–dacitic members. The basaltic patterns are transitional between typical calc-alkaline rocks and enriched MORB (E-MORB). Their transitional character between typical arc and mid-ocean ridge magmas is comparable to that of basalts formed in supra-subduction zone extensional regimes. Furthermore, their enriched nature makes the Debesa metabasalts remarkably similar to modern back-arc

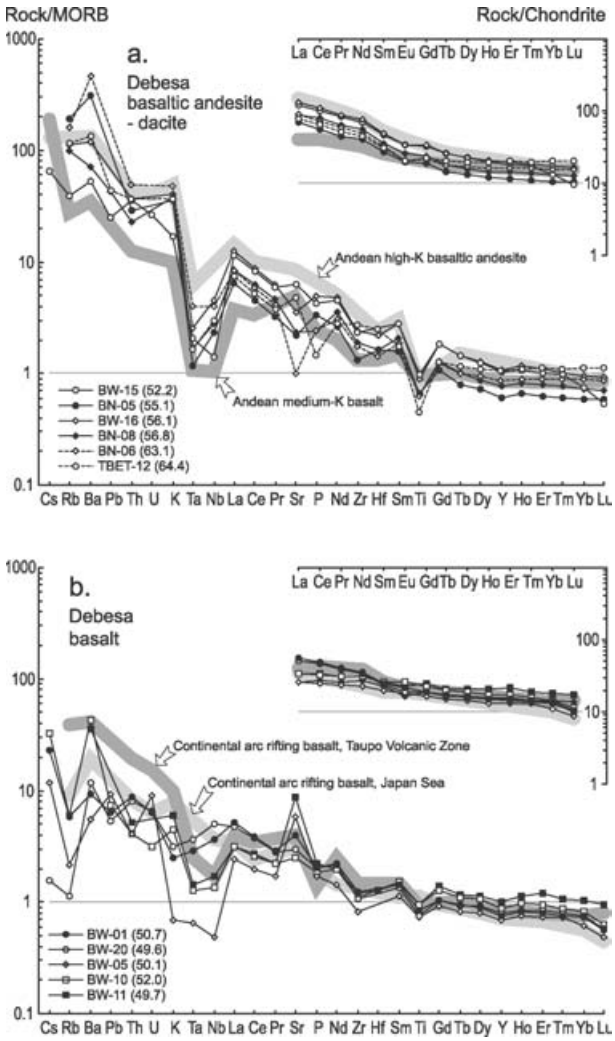

Figure 4. MORB-normalized spidergrams and chondrite-normalized REE plots of (a) Debesa metavolcanites of basaltic andesite to dacitic composition v. typical Andean margin medium-K basalt (dark grey; sample 1212764 from Tormey *et al.* 1991) and high-K basaltic andesite (light grey; sample cc5 from Kay *et al.* 1991) for comparison; (b) Debesa metabasalts v. continental arc rifting basalts from the Japan Sea (light grey; sample J-2b from Pouclet *et al.* 1995) and Taupo Volcanic Zone (dark grey; sample TVZ-17 from Gamble *et al.* 1993) for comparison. Normalizing values from Sun & McDonough (1989). SiO_2 contents for the analysed samples are shown in brackets.

basin or arc rifting basalts in regions where the concomitant arc is built on thin continental rather than on oceanic crust (e.g. Ewart *et al.* 1994; Pearce *et al.* 1995*a*; Petford & Atherton, 1995).

The mafic members of the Kilaj intrusive complex have varying trace element and REE spectra that largely overlap with the Debesa metabasalts, although the Kilaj rocks show less Th-enrichment compared to that of other highly incompatible elements (Fig. 5a). Some of the intermediate and felsic varieties show larger negative Nb–Ta anomalies and steeper MORB-normalized patterns that are more like those of the

https://doi.org/10.1017/S001675680300801X Published online by Cambridge University Press

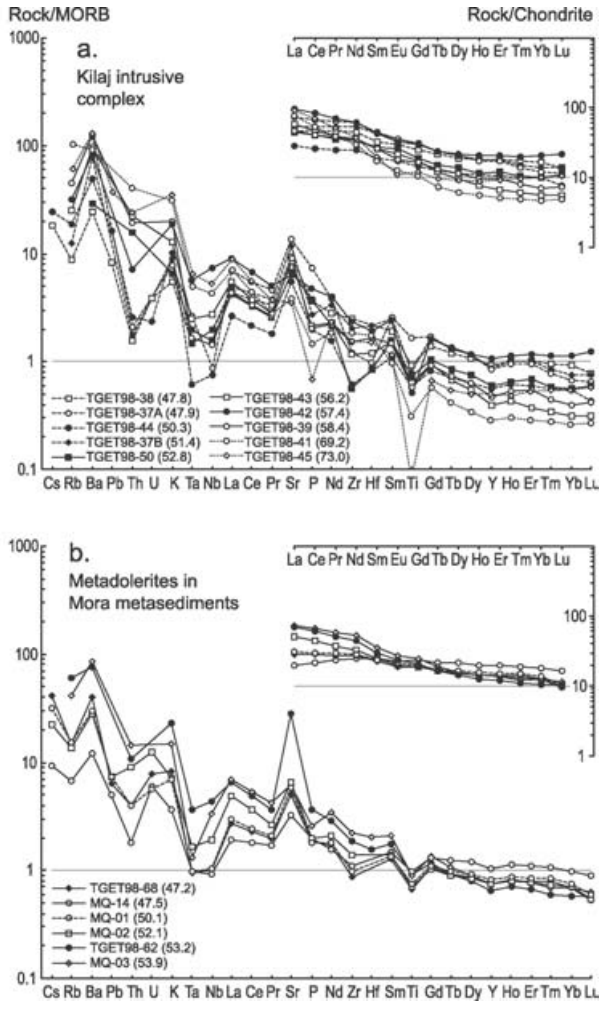

Figure 5. MORB-normalized spidergrams and chondrite-normalized REE plots of (a) the Kilaj intrusive complex; (b) dykes in Mora sedimentary sequence. SiO_2 contents for the analysed samples are shown in brackets.

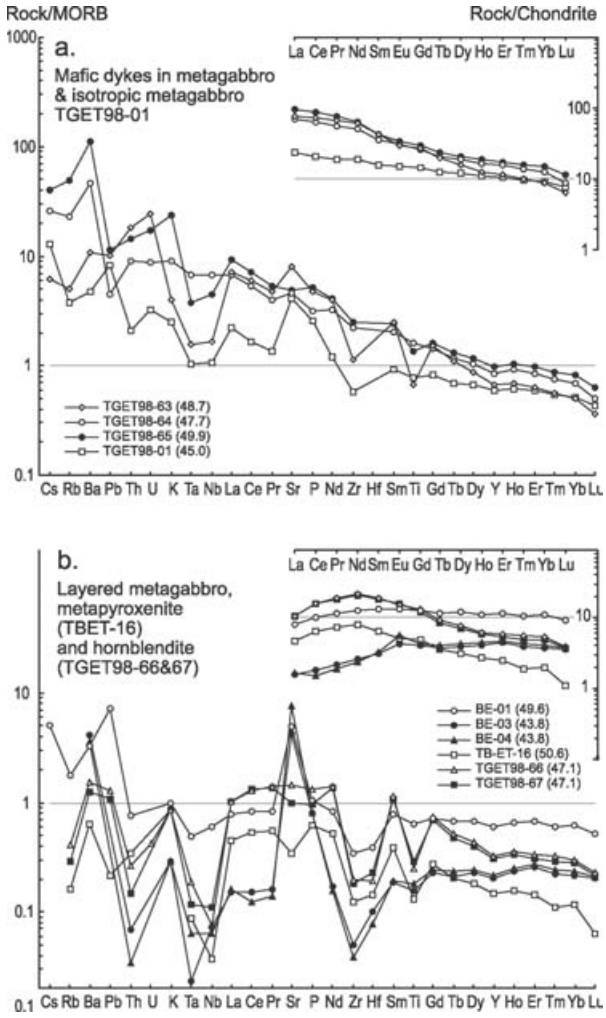

Figure 6. MORB-normalized spidergrams and chondrite-normalized REE plots of plutonic rocks in mafic–ultramafic complexes: (a) dykes and isotropic gabbro TGET98–01; (b) layered metagabbro, metapyroxenite and hornblendite. SiO_2 contents for the analysed samples are shown in brackets.

Debesa basaltic andesites and dacites. The LILE show strong enrichments that concur with the light rare earth element (LREE) enrichments, in accordance with the moderate metamorphic alteration and little mobilization of the LILE. Thus, the significant Ba and Sr anomalies are probably primary features of the magmas that are reflected also in many of the other pre-D_1 igneous rocks (Figs 4–6), although the anomalies are less consistent in the completely metamorphic volcanic rocks and sediment-hosted dykes.

The essentially mafic dykes in the Mora metasediments also have compositions that cover the range of MORB-normalized and REE patterns seen in the Debesa metabasalts, including their significant variation in negative Nb–Ta anomalies (Fig. 5b). Like the Kilaj complex, the dykes also include varieties with somewhat more fractionated trace element patterns, with a Th enrichment factor of up to 15 compared to MORB and La_N/Yb_N ratios up to 6. One sample is less enriched with a nearly flat, slightly convex REE pattern and a Th enrichment factor of less than 2 × MORB, although still with significant subduction signatures such as negative Nb–Ta and Ti anomalies.

The gabbroic to ultramafic plutonic rocks and their associated basaltic dykes show large variations in their trace element and REE spectra (Fig. 6). The limited number of dykes analysed have MORB-normalized and REE patterns (Fig. 6a) that are similar to the most enriched varieties of Debesa metabasalts and dykes in the Mora metasediments. One sample of isotropic metagabbro (TGET98-01) is broadly comparable to the least enriched Debesa metabasalts and Mora dykes, with La_N/Yb_N ratios of 2.6 and slightly inclined MORB-normalized patterns showing small but significant Nb–Ta anomalies (Fig. 6a). Layered metagabbros display marked Sr, Eu and P anomalies that reflect cumulus plagioclase and apatite.

https://doi.org/10.1017/S001675680300801X Published online by Cambridge University Press

5.c. Synkinematic plutons

The Dogi and Duksi complexes both cover a wide spectrum of SiO_2 contents (Table 2). Our data indicate the presence of two geochemically distinct groups that conform to modal subdivisions. The dioritic to quartz monzonitic members form a continuum of rocks ranging from mafic to *c*. 65 % SiO_2; intermediate varieties predominate. A scarcity of rocks in the 65–70 % SiO_2 interval separates these rocks from the granodiorites and granites. The two groups form clear calc-alkaline trends in an AFM plot (not shown). In spite of field evidence of contemporaneous emplacement and magma mingling of the two groups, non-linear element–SiO_2 relationships demonstrate that the compositional spectrum of the dioritic to quartz monzonitic varieties cannot be explained solely in terms of magma mixing. For example, Al_2O_3, Na_2O and K_2O contents are higher in intermediate than in mafic and felsic rocks (Table 2).

The dioritic to quartz monzonitic members of the plutons are rich in potassium and total alkalies. According to standard IUGS classification of igneous rocks (Le Maitre *et al.* 1989) these fine- to medium-grained and little altered intrusives cover a compositional range stretching from high-K basalt and potassic trachybasalt, through shoshonite and latite, to trachyte. In line with their potassic nature, they are characterized by extremely fractionated REE and MORB-normalized patterns (Fig. 7a). The latitic and trachytic varieties have La_N/Yb_N ratios of 23–36, and the most incompatible trace elements are enriched by a factor of 30–600 compared to MORB. Barium contents are in the order of 1500 to 3000 ppm and, particularly in the Duksi intrusives, show large peaks in the trace element patterns. Strontium shows similar enrichments. Negative Nb–Ta anomalies are typical in all varieties, although less distinctive in the Dogi than in the Duksi complex. The XRF data on a more comprehensive set of samples from the synkinematic intrusions indicate that La_N/Yb_N ratios may be as high as 100. Comparable patterns are found in the trachybasaltic and shoshonitic varieties.

The granodioritic to granitic varieties of the synkinematic plutons are moderately peraluminous with A/CNK values of 1.0 to 1.2, in accordance with their S-type affinity as indicated by the presence of muscovite and garnet in some varieties. They are characterized by moderate to strong enrichment of LREE, with La_N/Yb_N ratios between 7 and 95, and insignificant Eu anomalies (Fig. 7b). Contents of HREE are about one order of magnitude lower than in MORB, and also other incompatible HFSE are significantly depleted in comparison with the less leucocratic synkinematic types.

The steep REE patterns of the basaltic to trachytic synkinematic rocks, and their extreme enrichment of the highly incompatible trace elements coupled with varying Nb–Ta anomalies, are comparable to that of potassic rocks typical of continental collision regimes such as Turkey (Fig. 7a). The granodiorites and granites have low values of HREE and Nb–Ta similar to syn-collisional and volcanic arc granitoids. Although both the Duksi and the somewhat younger Dogi complex plot mainly within the field of 'volcanic arc granites' in Rb–Y–Yb–Nb–Ta discriminant diagrams (not shown), the Dogi granitoids have generally higher Rb and Nb–Ta contents (Table 2) that are close to those of the 'syn-collisional granites' of Pearce, Harris & Tindle (1984).

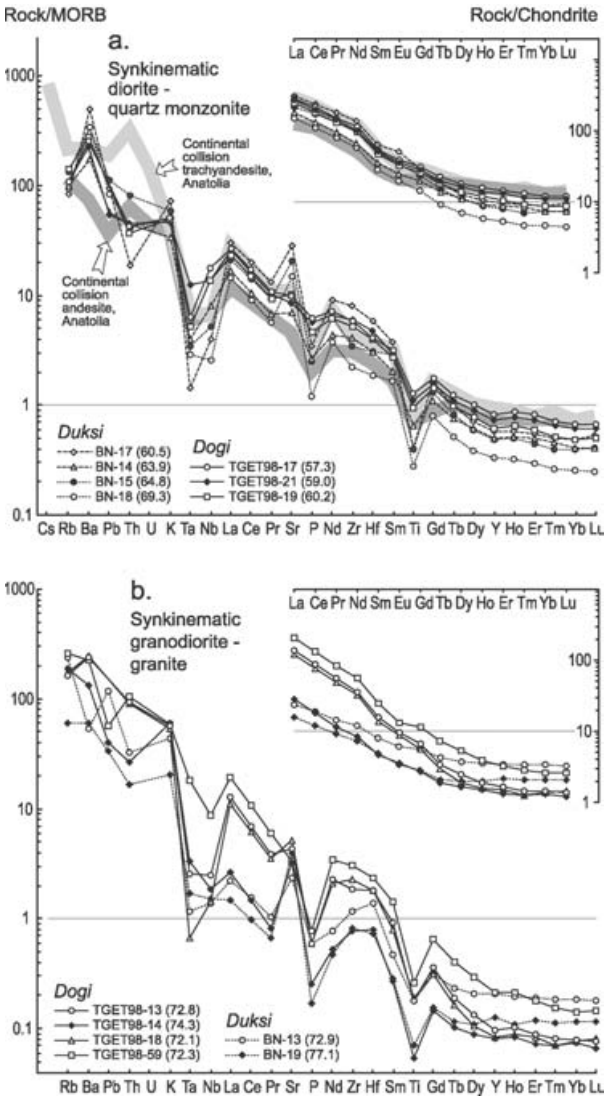

Figure 7. MORB-normalized spidergrams and chondrite-normalized REE plots of intrusive rocks from the Dogi and Duksi synkinematic composite plutons. (a) dioritic to quartz monzonitic rocks; (b) granodioritic and granitic rocks. Comparison with continent-collision related rocks from Turkey (light grey: Western Anatolian trachyandesite EA413 from Aldanmaz *et al.* 2000; dark grey: Eastern Anatolian andesite KARS2921 from Pearce *et al.* 1990). SiO_2 contents for the analysed samples are shown in brackets.

https://doi.org/10.1017/S001675680300801X Published online by Cambridge University Press

6. Isotope systematics

A set of 20 representative samples of metavolcanic and plutonic rocks have been analysed for Sr and Nd isotopes at the Department of Earth Sciences, Memorial University of Newfoundland, Canada (Table 3). Samples were dissolved with HNO_3–HF acids before being evaporated to dryness. Sr was first separated from the re-dissolved sample by specific extraction chromatography using EICHROM Sr resin and a procedure similar to that described by Pin *et al.* (1994). Rare earth elements were subsequently separated by specific extraction chromatography using EICHROM TRU-Spec resin before Nd was separated on Teflon columns using a procedure described by MacLachlan & Dunning (1998). The Sr and Nd separates were loaded on outgassed Re double filaments and analysed on a Finnigan MAT 262 mass-spectrometer using static faraday multicollector routines. The errors in $^{87}Sr/^{86}Sr$ and $^{143}Nd/^{144}Nd$ (Table 3) are reported at the 2-sigma (95 %) confidence levels and are based solely on mass spectrometry measurements.

The $^{87}Sr/^{86}Sr$, $^{143}Nd/^{144}Nd$ initial ratios, ε_{Sr} and ε_{Nd} were calculated using the ages from U–Pb geochronology (see Section 4) and the contents of Rb, Sr, Sm and Nd as analysed by ICP-MS and XRF (Table 3). Values for the Debesa metavolcanites and the pre-D_1 dykes in the Mora metasediments were calculated using an inferred age (866 Ma) based on the geochemical similarity and supposed correlation with the Kilaj complex.

The initial $^{87}Sr/^{86}Sr$ values for the Debesa metavolcanites vary from 0.7018 to 0.7034 (Fig. 8); the two samples of andesite have Sr-isotope values close to the MORB-type depleted mantle beneath northeastern Africa, as introduced by Stern & Hedge (1985). The other pre-D_1 rocks have higher initial $^{87}Sr/^{86}Sr$ values between 0.7028 and 0.7042. For the metavolcanites and sediment-hosted metadolerites where the mineralogy is purely metamorphic, the high ε_{Sr} could possibly be explained by seawater alteration, however, this explanation is less likely in the case of the only moderately altered Kilaj intrusives, which in fact show the greatest deviation from the mantle value (Fig. 8).

The data from the volcanic suite form an errorchron in the Rb–Sr diagram of 873 ± 82 Ma (Fig. 9), overlapping with the U–Pb zircon age from the Kilaj complex. The initial $^{87}Sr/^{86}Sr$ value is 0.7027 ± 0.0016, which falls within the range for the depleted mantle by Stern & Hedges (1985).

The initial $^{143}Nd/^{144}Nd$ values for the Debesa metavolcanites vary from 0.51173 to 0.51187, corresponding to ε_{Nd} (t = 866 Ma) values between +4.1 to +6.8. These values are in the range of, and lower than, the depleted mantle value of ε_{Nd} (t = 866 Ma) = +6.1 as calculated according to the model by Nelson & DePaolo (1985). They are comparable to the isotopic values from continental arcs underlain by a relatively thin and young crust, such as the northern and parts of the southern volcanic zones of the Andean margin (e.g. Kay *et al.* 1991; Tormey *et al.* 1991) and the Taupo Volcanic Zone in New Zealand (Gamble *et al.* 1993). They also overlap with those of typical oceanic island arc/back-arc volcanic rocks (e.g. Hawkesworth *et al.* 1979; Nohda & Wasserburg, 1981).

The andesitic and dacitic samples have $^{147}Sm/^{144}Nd$ ratios below 0.16 and may therefore be used to calculate model ages according to the depleted mantle model, T_{DM}, by Nelson & DePaolo (1985). The model ages

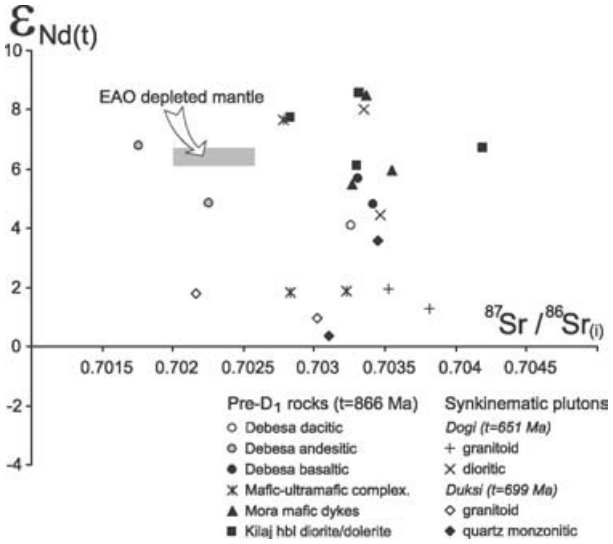

Figure 8. Initial $^{87}Sr/^{86}Sr$ v. ε_{Nd} diagram for pre-D_1 volcanic and intrusive rocks and synkinematic plutons from Western Ethiopia. Shaded area is the isotopic composition of depleted mantle beneath the East African Orogen (EAO). The Sr mantle range is from Stern & Hedge (1985), while the Nelson & DePaolo (1985) mantle model has been used for the range in ε_{Nd} values in accordance with Stern & Abdelsalam (1998) and Stern (2002).

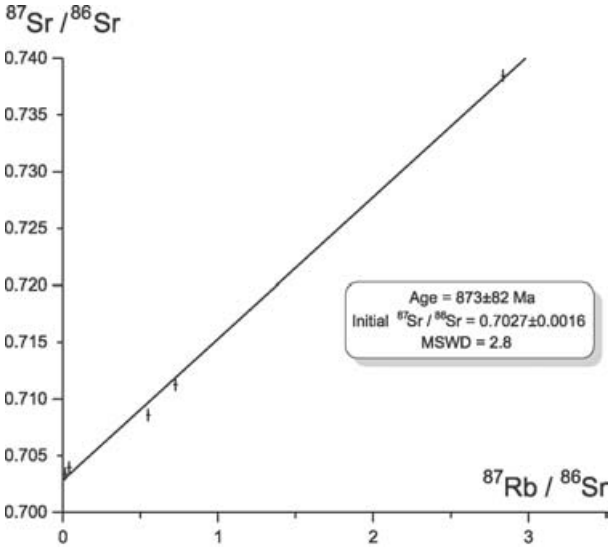

Figure 9. Rb–Sr errorchron diagram for the Debesa metavolcanic rocks (data set in Table 3). Data-point error crosses are 1σ.

https://doi.org/10.1017/S001675680300801X Published online by Cambridge University Press

Table 3. Sr and Nd isotope data for igneous rocks of the East African Orogen in Western Ethiopia; analytical procedures are given in the text

Sample no.	Rock	Unit	Age (Ma)	$^{87}Sr/^{86}Sr$	$^{143}Nd/^{144}Nd$	Rb*	Sr*	Sm*	Nd*	$^{87}Rb/^{86}Sr$	$^{87}Sr/^{86}Sr(i)$	$^{143}Nd/^{144}Nd(i)$	$\varepsilon_{Nd}(t)$	$^{147}Sm/^{144}Nd$	$\varepsilon_{Nd}(0)$	T_{DM}
TGET98-13	Granitoid	Dogi	651	0.709946(18)	0.512237(56)	*92*	*389*	2.4	16.7	2.838	0.70381	0.511865	1.3	0.08732	−7.8	975
TGET98-18	Granitoid	Dogi	651	0.708931(36)	0.512267(16)	*98*	*470*	2.2	15.4	0.726	0.70352	0.5119	2.0	0.08593	−7.2	930
TGET98-19	Monzodiorite	Dogi	651	0.705580(17)	0.512619(39)	*78*	*909*	7.1	44.7	0.551	0.70335	0.512211	8.0	0.09571	−0.4	563
TGET98-21	Monzodiorite	Dogi	651	0.705523(32)	0.512445(23)	*60*	*760*	7.7	47.5	0.007	0.70347	0.512029	4.5	0.09784	−3.8	794
BN-13	Granitoid	Duksi	700	0.720647(24)	0.512391(16)	*132*	*209*	1.2	5.6	0.042	0.70302	0.511787	1.0	0.13190	−4.8	1214
BN-19	Granitoid	Duksi	700	0.704780(35)	0.512436(13)	*34*	*362*	0.7	3.4	0.662	0.70216	0.51183	1.8	0.13245	−3.9	1139
BN-14	Quartz monzonite	Duksi	700	0.705579(21)	0.512225(10)	*55*	*618*	5.4	31.7	0.584	0.7031	0.511757	0.4	0.10246	−8.1	1122
BN-17	Quartz monzonite	Duksi	700	0.703970(25)	0.512340(26)	*47*	*2533*	9.8	65.0	0.240	0.70345	0.511922	3.6	0.09145	−5.8	882
BN-06	Metadacite	Debesa	866	0.738462(17)	0.512474(17)	*91*	*90*	4.9	22.6	0.221	0.70326	0.511727	4.1	0.13130	−3.2	1055
BN-08	Metaandesite	Debesa	866	0.711257(13)	0.512485(20)	*55*	*212*	5.5	26.2	1.770	0.70225	0.511766	4.8	0.12642	−3.0	978
BW-16	Metaandesite	Debesa	866	0.708589(12)	0.512588(26)	*63*	*320*	7.4	35.1	0.263	0.70176	0.511866	6.8	0.12694	−1.0	809
BW-05	Metabasalt	Debesa	866	0.703394(34)	0.512778(24)	1.2	511.6	2.9	10.5	0.249	0.70331	0.511809	5.7	0.17025	2.7	
BW-10	Metabasalt	Debesa	866	0.703947(8)	0.512738(19)	3.3	218.0	4.0	14.3	0.052	0.70342	0.511765	4.8	0.17092	2.0	
MQ-01	Metadolerite	Mora	866	0.703958(36)	0.512879(46)	8.7	508.0	3.6	13.2	0.059	0.70337	0.511953	8.5	0.16269	4.7	
MQ-03	Metadolerite	Mora	866	0.704722(25)	0.512557(33)	*23*	*550*	5.5	24.8	0.017	0.70327	0.511799	5.5	0.13317	−1.6	926
MQ-14	Metadolerite	Mora	866	0.704029(18)	0.512965(71)	3.7	273.5	3.8	11.5	0.089	0.70355	0.511824	6.0	0.20046	6.4	
TGET98-38	Metadolerite	Kilaj	866	0.704399(20)	0.512703(19)	5.0	817.6	5.0	20.5	0.051	0.70419	0.511862	6.7	0.14787	1.3	800
TGET98-44	Metadolerite	Kilaj	866	0.703562(10)	0.512800(14)	10.6	498.8	2.9	11.3	0.048	0.70283	0.511914	7.7	0.15575	3.2	662
TGET98-42	Metaquartzdiorite	Kilaj	866	0.704400(17)	0.512593(60)	*18*	*566*	6.4	28.8	0.117	0.7033	0.511831	6.1	0.13374	−0.9	866
TGET98-43	Metadiorite	Kilaj	866	0.703946(21)	0.512768(50)	*14*	*772*	4.0	16.8	0.038	0.70332	0.511956	8.6	0.14260	2.5	611
TGET98-66	Hornblendite	Mafic-ultramafic	866	0.702887(17)	0.512613(25)	0.2	126.9	2.9	10.0	0.007	0.70283	0.511611	1.8	0.17606	−0.5	
TGET98-67	Hornblendite	Mafic-ultramafic	866	0.702842(8)	0.512893(33)	0.2	84.8	2.8	9.7	0.005	0.70278	0.511909	7.6	0.17279	5.0	
BE-01	Metagabbro	Mafic-ultramafic	866	0.703315(10)	0.512758(13)	1.0	399.6	2.0	5.9	0.005	0.70323	0.511614	1.9	0.20109	2.3	

Data in italics from XRF, otherwise ICP-MS. * = contents in ppm. 2σ uncertainties in Sr and Nd ratios shown in parentheses (last 2 digits). $\varepsilon_{Nd}(t)$ calculated for the tabulated ages. $^{146}Nd/^{144}Nd = 0.7219$ corresponds to $^{143}Nd/^{144}Nd_{CHUR} = 0.512638$. $^{87/86}Sr(i)$ and $^{143/144}Nd(i)$ initial values calculated for the tabulated ages. T_{DM} model ages are according to Nelson & DePaolo (1985), calculated for samples with $^{147}Sm/^{144}Nd < 0.16$.

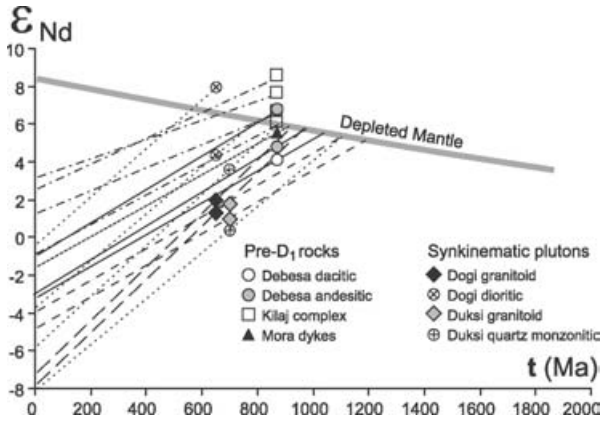

Figure 10. ε_{Nd}–T diagram with model ages for pre-D_1 volcanic and intrusive rocks and synkinematic plutons from Western Ethiopia. See text for details.

range from 60 Ma younger, to nearly 200 Ma older, than the U–Pb zircon age of 866 Ma (Table 3). In the ε_{Nd} v. T diagram the data points are close to the depleted mantle curve, suggesting that the metavolcanites represent pristine mantle material only weakly contaminated by older crustal material.

Calculated ε_{Nd} (t = 866 Ma) values for the Mora dykes and Kilaj complex are +5.5 to +8.5 and +6.1 to +8.6, respectively. These values are in the upper range of, or slightly higher than, values for the metavolcanites (Fig. 8). One sample from a Mora dyke and two from the Kilaj complex give T_{DM} model ages close to the metavolcanites (Table 3). The other two Kilaj samples give model ages of 611 and 662 Ma, which indicate that they are more depleted than the mantle model (Fig. 10) and point to a possible involvement of a different mantle source or fractionation during crustal remelting and differentiation of the melt.

The synkinematic intrusions show significant isotopic variations. The granodiorites and granites from both complexes have uniform ε_{Nd} values between 1.0 and 2.0 (Table 3). Dioritic and quartz monzonitic rocks from Duksi and Dogi have ε_{Nd} values of 0.4–3.6 and 4.5–8.0, respectively. As for the metavolcanic and subvolcanic units, the Sr isotope values show a large spread (initial $^{87}Sr/^{86}Sr$ of 0.7022 to 0.7038) and correspond only poorly to the Nd isotopic variations.

In the ε_{Nd}–T diagram, the Duksi and Dogi granitoid members show different evolution lines and T_{DM} ages, suggesting that the sources for these granites are different (Fig. 10). The *c*. 700 Ma Duksi granitoids have model ages of 1100–1200 Ma, which are similar to the model age of 1130 Ma presented by Stern (2002) for southern Ethiopia. In contrast, the source for the 651 Ma Dogi granitoids comes out with model ages of 800–900 Ma, which is similar to the age of the bulk of pre-D_1 igneous rocks in the region. The formation of the dioritic and quartz monzonitic members apparently involved 900–1100 Ma crustal material in the case of Duksi and apparently 600–800 Ma crustal material in the case of Dogi, both conforming broadly to the results for the respective granitic rocks.

7. Discussion

7.a. Pre-D_1 development: continental margin arc and arc rifting?

The Debesa metavolcanites have many features in common with mature arcs, including the great abundance of intermediate to felsic calc-alkaline volcanic rocks. The presence of interlayered tuffaceous sediments, conglomerates and carbonate breccias, coupled with the local existence of pillowed lavas, are suggestive of a marine environment. Parts of this marine setting must have been shallow to account for the high vesicularity of some lava flows, while graphitic sediments were probably deposited in restricted and possibly deeper parts of the marine basins. Nevertheless, the profusion of pyroclastic deposits signifies a major input to the volcanic-sedimentary record derived from subaerial volcanism. A plausible depositional setting for these mixed lithologies would be that of carbonate reef-fringed volcanic islands separated by marine, partly anoxic, basins.

The highly evolved, high-K to medium-K, calc-alkaline nature of the intermediate and felsic members of the Debesa metavolcanites is typical of active continental margin magmatism. The most prominent example of this setting is the Andean front, but similar rocks are characteristic of volcanic arcs built on thinner continental crust such as the Taupo Volcanic Zone on New Zealand and the Banda Arc and the Flores–Java–Sumatra arc segments of Indonesia (e.g. Gamble *et al.* 1993; Honthaas *et al.* 1998; Carn & Pyle, 2001). High-K to medium-K calc-alkaline rocks can be found also in mature oceanic arcs, however, in the latter setting they are less common and rarely show the strong enrichment in highly incompatible trace elements (see, e.g. Pearce, 1983; Pearce & Peate, 1995) as seen in the Debesa sequence.

Mafic members of the Debesa sequence contrast with the intermediate to felsic metavolcanites in their less enriched and more variable REE patterns, and their inconsistent and generally smaller negative Nb–Ta anomalies. Significant differences in incompatible-element ratios show that the two groups were not petrogenetically related by fractional crystallization. This is valid also for variations among the basaltic members, implying either a heterogeneous mantle source or varying components of crustal contamination. Comparable mafic magmas can be found in some Large Igneous Provinces (LIPs), in particular those of continental affinity. Stein & Goldstein (1996) proposed a LIP model for rapid formation of Arabian–Nubian Shield crust between *c*. 875 and 725 Ma by voluminous oceanic plateau magmatism from a plume

https://doi.org/10.1017/S001675680300801X Published online by Cambridge University Press

head, succeeded by calc-alkaline magmatism at a convergent margin. However, this model does not apply to the presently studied part of the Arabian–Nubian Shield, because the basaltic units are only subordinate and are interlayered with large amounts of intermediate and felsic, largely pyroclastic, rocks that are atypical of LIPs (e.g. Saunders *et al.* 1996).

The transitional character of the mafic lavas, having partly calc-alkaline and partly enriched MORB-like geochemical signatures, fits best with a continental back-arc or rifted-arc palaeotectonic setting as noted in Section 5.b. Available data from modern settings show comparably enriched trace element patterns in basalts related to arc extension in New Zealand (Gamble *et al.* 1993) and back-arc basin opening in the Japan Sea and the Banda Arc (Ujike & Tsuchiya, 1993; Pouclet *et al.* 1995; Honthaas *et al.* 1998), while even stronger enrichments of highly incompatible trace elements characterize arc extensional volcanites of the Andean arc (e.g. Petford & Atherton, 1995; Vergara *et al.* 1995).

The primary interdigitation of the mafic lava flows with the intermediate to felsic pyroclastites and associated sediments implies a temporal overlap between the two volcanic members. Since submarine basalts cannot flow large distances from their effusive vent sites, it can also be argued that basaltic volcanism within the basins was to some extent spatially separated from subaerial andesitic and dacitic eruptions on adjacent volcanic islands, even though some spatial overlap is demonstrated by the local occurrence of andesitic flows in the volcanic–sedimentary sequence.

Irrespective of the local volcanic and sedimentary milieu, in a palaeotectonic context the stratigraphic relationships between the two different members of the Debesa metavolcanites are suggestive of arc development and contemporaneous rifting or extension in a continental margin setting. Such a scenario would be broadly analogous to the syn-subduction crustal extension that was common along the Andean margin from the Jurassic to the Tertiary (e.g. Miller *et al.* 1994; Petford & Atherton, 1995; Vergara *et al.* 1995) and similarly in the southwest U.S. Cordillera in Early Mesozoic times (Riggs & Busby-Spera, 1990). A comparable setting was that of the initial extension of the proto-Japan island arc, which was situated on the margin of the Eurasian continent prior to opening of the Japan Sea in the Oligocene (Pouclet *et al.* 1995; Tamaki, 1995).

The ε_{Nd} ($t = 866$ Ma) values of $+4.1$ to $+6.8$ for the Debesa metavolcanites are compatible with (although not strictly diagnostic of) a model of arc development and rifting on a thin continental crust that had only a weak influence on the Nd isotope signatures. Similar ε_{Nd} values are found in the Northern and Southern Volcanic Zone in the Andes Region, South America (Kay *et al.* 1991; Lòpez-Escobar, Tagiri & Vergara, 1991), while the Central Volcanic Zone, where the continental crust is thicker and older, is characterized by significantly lower ε_{Nd} values (Kay *et al.* 1991). A similar pattern is also seen where the oceanic Kermadec arc passes into the Taupo Volcanic Zone that is underlain by the relatively thin and young continental crust of New Zealand. In that area, the ε_{Nd} drops from $+7$–8 to $+2$–3 with increasing continental influence towards New Zealand (Gamble *et al.* 1993). Comparable Nd isotope compositions characterize arc and arc-rifting volcanic rocks of the Banda Sea where thin continental crust is also present (Vroon *et al.* 1993; Honthaas *et al.* 1998).

Field observations of the substratum to the Debesa volcanic sequence are lacking. Thus the question of a possibly continental basement must rely on indirect evidence. The sediment-hosted dykes of the Mora sequence are of particular interest in this respect, in view of their striking geochemical and isotopic similarity to the Debesa metavolcanites (see Sections 5.b and 6). Braathen *et al.* (2001) interpreted the association of thick carbonates and arkosic or quartzitic sandstones with local conglomerates to suggest a shallow marine platform environment for the Mora sequence, analogous to that typical of passive continental margins or intracratonic seas. Moreover, these units are comparable to sedimentary successions underlain by high-grade gneisses in Sudan and Kenya, which have been interpreted to represent a passive margin sequence deposited along the eastern edge of West Gondwanaland subsequent to break-up of Rodinia at *c*. 900 Ma (Stern, 1994).

If the correlation of the Debesa metavolcanic rocks and the Mora dykes is valid, it strongly supports a continental setting for the arc and arc-rifting magmatism. In this model, the Mora sequence would be the equivalent of the arc basement, and the sediment-hosted dykes are representatives of the feeder system to the Debesa metavolcanic succession as suggested by Braathen *et al.* (2001). Interestingly, the Mora dykes show the greatest resemblance to the mafic, possibly arc rift-related, members of the metavolcanites. This is in accordance with the existence of dyke swarms suggestive of dilation-related magma supply in parts of the Mora sequence.

Yielding ages of about 860 Ma, our U–Pb zircon data and whole-rock Rb–Sr errorchron demonstrate that the Debesa metavolcanites are among the oldest arc-related sequences hitherto documented in juvenile Arabian–Nubian Shield terranes. Comparable ages have been reported for metavolcanic rocks of marginal basin affinity in the southeastern parts of the Sudanese Red Sea Hills (*c*. 850 Ma: Kröner *et al.* 1991) and for a calc-alkaline volcanic sequence of oceanic arc affinity in the Nakfa region (*c*. 854 Ma: Teklay, Kröner & Mezger, 2002). The age is only 40 Ma younger than the inferred opening of the 'Mozambique Ocean' at *c*. 900 Ma (Stern, 1994) and implies that the earliest stages of plate convergence may have taken place along an active

https://doi.org/10.1017/S001675680300801X Published online by Cambridge University Press

continental margin, and not exclusively in oceanic arcs as suggested in most previous models (see Blasband *et al.* 2000, and references therein). This apparent discrepancy could be accounted for by along-arc crustal variations, from oceanic-type crust in northern parts of the East African Orogen where most previous studies have been carried out, to continental-type crust in southern regions. Modern analogues to such a scenario are the transition from oceanic to continental arc along the Kermadec Islands–Taupo Volcanic Zone (New Zealand) convergent margin (Gamble *et al.* 1993) and the Flores–Java–Sumatra arc segments of Indonesia (Carn & Pyle, 2001).

The age of the Kilaj intrusive complex overlaps with that of the Debesa sequence and, like the Mora dykes, the complex shows remarkable similarities to the metavolcanites. This lends support to the interpretation of Braathen *et al.* (2001), who suggested that the Kilaj complex represents a part of the subvolcanic feeder system. Petrological and geochemical characteristics provide some information on the nature of this early record of calc-alkaline magmatism in the East African Orogen. The presence of hornblende as a primary phase at Kilaj indicates that the magma chamber crystallized at a depth of more than 25 km (Green, 1982), which requires the presence of a thickened crust at the time of emplacement. This is in agreement with the strongly fractionated REE patterns of parts of the Kilaj intrusion and of the Debesa basaltic andesites. For modern Andean lavas it has been argued that REE fractionation serves as a measure of crustal thickness (e.g. Kay *et al.* 1991; Tormey *et al.* 1991). The La/Yb ratios of the Debesa basaltic andesites cluster at *c.* 10, which is similar to parts of the comparatively thin Southern Volcanic Zone of the Andean margin, where crustal thickness is in the order of 30–40 km.

The existence of highly resorbed garnet in leucocratic parts of the Kilaj intrusion suggests that some of the more evolved magmas were derived from melting of, or contamination by, crustal material at greater depth. Thus, a possible model might include the interaction of crustal material and mafic magma derived by partial melting of a subduction-modified mantle wedge, similar to commonly accepted models for active continental margin magmatism (see, e.g. Wilson, 1989, and references therein).

The Sr isotope values of the Debesa metavolcanites, the Mora dolerites and the Kilaj complex are all shifted towards anomalously high values, considering the range in Nd isotope values (Fig. 8). One possible explanation is contamination from the Mora carbonates, which would cause high Sr isotope values without affecting the Nd isotopes. The carbonates have $^{87}Sr/^{86}Sr$ ratios of *c.* 0.7058 (unpub. data). Calculations show that 15–20 % carbonate is needed to shift the $^{87}Sr/^{86}Sr$ (t = 866 Ma) value to around 0.7033, if the pristine magma had 250 ppm Sr with a $^{87}Sr/^{86}Sr$ (t = 866 Ma) value of 0.7021, and the carbonate contained 750 ppm Sr with a $^{87}Sr/^{86}Sr$ (t = 866 Ma) value of 0.70581. If the carbonate successions included evaporite beds, which would be higher in Sr (1500–2000 ppm), the contamination could be down to 5 %.

The prominent Ba and Sr peaks in the trace element patterns for the Kilaj complex and, less consistently, in the metamorphic volcanic rocks and sediment-hosted dykes, are interesting in this regard. Ba and Sr enrichments are characteristic of subduction-related magmas in general and are generally attributed to metasomatism of their mantle source region by hydrous fluids derived from the subducted oceanic crust (e.g. Wilson, 1989), however, they are generally accompanied by similar enrichments of other incompatible LILE. Thus it is likely that the Ba and Sr spikes observed here reflect comparable anomalies either in their mantle source region or in crustal contaminants. Rocks that have the capacity of providing significant amounts of these elements are evaporates (Ba and Sr), carbonates (Sr) and bedded barite. Evaporite beds appear to have been widespread in Proterozoic sequences elsewhere (Kah, Lyons & Chesley, 2001), and bedded barite associated with iron formations has been described from Precambrian rocks of Western Ethiopia (De Wit, 1981). Although the effect of such contaminants on the magmas can hardly be documented, the conspicuous enrichments of Ba and Sr coupled with high ε_{Sr} values in little-altered rocks is clearly in favour of this model. The argument is supported by consistently similar trace element and isotopic patterns for the much younger synorogenic intrusions at Dogi and Duksi.

7.b. The ophiolite/suture enigma

The gabbroic to ultramafic complexes of the region, along with the similar complexes at Tulu Dimtu and Yubdo and further north, have generally been regarded as ophiolite fragments and have been taken to imply the presence of regional suture zones. However, as noted by Braathen *et al.* (2001), no units that are generally considered essential for the identification of ophiolites, such as tectonized mantle harzburgite, sheeted dyke complex, or basaltic pillow lavas with associated pelagic sediments, have been documented as being directly associated with these complexes. Harzburgitic varieties may have been included in the complexes, however, the presence of harzburgite is not by itself diagnostic of ophiolites since they are also commonly found in layered intrusions (e.g. McBirney, 1993). Moreover, the erratic distribution of the ultramafites is problematic in light of the suture model.

It is obvious that the compositions of mafic–ultramafic complexes like these have been greatly influenced by cumulate processes. Hence, geochemical data must be treated with caution because major and trace element ratios and concentrations may be far from

https://doi.org/10.1017/S001675680300801X Published online by Cambridge University Press

their related melts. Isotropic metagabbros analysed in the present study have compositions that may be near original melt compositions although they still show geochemical signatures reflecting the presence of cumulus phases. Cogenetic dykes are likely to be compositionally closer to melt compositions. Interestingly, the gabbro- and ultramafite-related dykes have geochemical fingerprints that overlap with the subduction-related patterns of other pre-D_1 metavolcanites and possible subvolcanic intrusions, including marked LREE and LIL enrichments coupled with a variable but significant depletion in Nb–Ta and TiO_2 (Fig. 6a). This is supported by Nb–Ta depletions also in gabbroic and ultramafic rocks (Fig. 6b), although these are cumulates and cannot be compared directly with rocks representing melt compositions.

The chemical composition of the mafic–ultramafic complexes and associated dykes does not in itself exclude an ophiolitic origin. In fact, most ophiolites worldwide have proved to have a supra-subduction zone affinity, and this is noted also by Stern (1994) as an argument for a back-arc origin for ophiolites of the East African Orogen in general. Nevertheless, the striking similarity between gabbro-ultramafite-hosted dykes on one side, and metasediment-hosted dykes, Kilaj intrusive rocks and parts of the Debesa sequence on the other side is intriguing and hints at a genetic link. In particular, the abundance of primary hornblende in gabbroic to ultramafic cumulates, and the association of hornblende-bearing gabbros with local ultramafites in the Kilaj complex, point to a common origin. Interestingly, the presence of hornblenditic cumulates has been noted also in mafic–ultramafic complexes of supposedly ophiolitic origin further north, in the Axum area in Ethiopia (Tadesse, Hoshino & Sawada, 1999). The evidence of hornblende crystallization implies that the ultramafites and associated gabbros were emplaced at depth in a crust considerably thicker than typical oceanic crust as represented by ophiolites.

Previous studies seem to have overemphasized the point that ultramafic complexes in the region are aligned along regional shear zones. Although this may be true to some extent, such as along the Baruda shear belt that appears to stretch south towards Tulu Dimtu and Yubdo, it is quite obvious that numerous similar complexes are rather erratically distributed elsewhere in the region (Fig. 2). The majority of these ultramafites seem to be located in metasedimentary lithologies that are, as pointed out by Braathen *et al.* (2001), comparable to that of the Mora sequence. Contacts to the metasediments are highly sheared and do not reveal any evidence of primary intrusive relations, yet we consider it highly unlikely that the spatial and geochemical relationships to the sediment-hosted dykes are pure coincidence.

On the basis of our combined data, a more appealing model for the mafic–ultramafic complexes is the emplacement of solitary intrusions. In response to penetrative D_1 deformation, the intrusions were later tectonically modified and partly aligned along regional shear zones. The intrusive bodies may also have had a significant controlling effect on the localization of shear zones due to competence contrast to the surrounding sedimentary lithologies, as suggested by Braathen *et al.* (2001).

At any rate, early rift-related magmatism is implied by the presence of dyke swarms in parts of the Mora sequence. The geochemical data on the intrusive complexes and dykes is suggestive of back-arc or within-arc extension in a continental margin setting. Whether dilation was locally sufficient to yield true oceanic crust, a prerequisite for a meaningful application of the term 'ophiolite' (e.g. Coleman, 1977; Nicolas, 1989; Gass, 1990), is at best doubtful for this part of the orogen. A more likely model includes the supply of mantle-derived melts into local magma chambers and dyke swarms in response to only limited dilation contemporaneous with subaerial arc magmatism nearby. This is not in conflict with the possible existence of true ophiolites, which may well have developed by more extensive arc or back-arc rifting further north in the East African Orogen.

7.c. Synkinematic magmatism and the closure of the 'Mozambique Ocean'

Recent models for the generation of orogenic composite intrusions, like those at Duksi and Dogi, generally count on a combination of mantle and crustal processes for the mafic and felsic components, respectively (e.g. Barbarin, 1999). Essential in most models is an inferred partial melting of enriched sub-continental mantle modified by pre-collision subduction events (e.g. Pearce *et al.* 1990; Keskin, Pearce & Mitchell, 1998), a process which explains why many of the typical subduction zone fingerprints, such as negative Nb–Ta anomalies and LILE enrichments, are retained in mafic to intermediate collisional magmas. Furthermore, the large preponderance of intermediate to felsic rocks in orogenic plutons has generally been considered as compelling evidence for extensive interaction between mantle-derived melts and crustal rocks, including large-scale melting caused by underplated mafic melts at the base of the crust (see, e.g. Bellieni *et al.* 1996, and references therein).

The syntectonic intrusions at Duksi and Dogi were clearly coeval with the main, orogenic, D_1 phase of deformation (Braathen *et al.* 2001). Yielding a U–Pb titanite age of 651 ± 5 Ma, interpreted to be close that of crystallization of the pluton, the age of the Dogi batholith is identical within uncertainty to the age of 640 ± 20 Ma suggested by Meert (2003) for continent collision and final closure of the 'Mozambique Ocean'. The zircon age of 699 ± 2 Ma for the Duksi intrusion provides evidence of somewhat earlier crystallization. According to recent models for the development of the

https://doi.org/10.1017/S001675680300801X Published online by Cambridge University Press

East African Orogen, the latter is within a period of arc accretion that started at *c*. 750 Ma and that gave way to the collisional event after *c*. 670 Ma (Blasband *et al.* 2000; Meert, 2003). Since there is no field evidence of separate deformational histories for the two plutons (Braathen *et al.* 2001) the span in ages may be interpreted in two ways: (1) arc accretion and subsequent continent collision were elements of a more or less continuous tectonic phase lasting 50 Ma or more, or (2) a long-lasting continent collision phase started earlier than previously thought. The latter model is most appealing in view of the remarkable similarity of the two complexes.

The few mafic, and abundant shoshonitic, latitic and trachytic rocks of both intrusions have geochemical characteristics that are typical of continental collision zones such as the Anatolian volcanic province of Turkey (Keskin, Pearce & Mitchell, 1998; Aldanmaz *et al.* 2000). Moreover, their extremely steep REE patterns and comparatively low contents of HREE may suggest a garnet-bearing mantle source, as argued by Aldanmaz *et al.* (2000) for late-orogenic, alkaline, basaltic rocks of the Anatolian volcanic province. This is in accordance with a model of magma generation under a thick lithospheric cap where one might expect melting to be restricted to the garnet lherzolite facies (Pearce & Parkinson, 1993). The REE patterns of granodioritic and granitic members of the composite intrusions also signify the presence of residual garnet in the source, and this is substantiated by the presence of resorbed garnet at Duksi. Analogous to moderately peraluminous granitoids elsewhere, their composition may be ascribed to partial melting of garnet-bearing rocks in the lower crust. The large spread in Sr isotope values coupled with significant Sr and Ba anomalies may suggest variable crustal contamination by carbonates and/or evaporates with high $^{87}Sr/^{86}Sr$ ratios as argued above for the pre-D_1 volcanic and intrusive rocks.

The Nd isotope values are in the upper range for collision-related volcanic rocks in Turkey, which have been interpreted to reflect crustal contamination of mantle-derived magmas (Pearce *et al.* 1990; Aldanmaz *et al.* 2000). The slight increase in ε_{Nd} values from the quartz monzonitic members of the *c*. 700 Ma Duksi intrusion (ε_{Nd} 0.4–3.6) to the dioritic members of the 651 Ma Dogi pluton (ε_{Nd} 4.5–8.0) can be interpreted to result from reduced crustal assimilation, because the variation coincides with lower SiO_2 contents. A somewhat similar increase in ε_{Nd} values in western Anatolian lavas has been ascribed to progressive crustal thinning since the early stage of collision-related volcanism in the Early Miocene (Aldanmaz *et al.* 2000). This model involves a shift from compressional to extensional tectonics and is perhaps not strictly applicable to the Duksi and Dogi complexes, because our data indicate that both intrusions were emplaced in a similar compressional tectonic regime.

At any rate, the comparatively primitive Nd isotope signatures, and the young model ages (T_{DM} of 800–1200 Ma) of the Duksi and Dogi complexes, combined with the arc-like signatures for the granodioritic to granitic members in Rb–Y–Yb–Nb–Ta discriminant diagrams of Pearce, Harris & Tindle (1984), can be interpreted in terms of contamination and melting processes in a collision zone dominated by juvenile crust such as accreted arc terranes. Interestingly, our model ages correspond well with those calculated by Stern (2002) based on existing Nd isotopic data from northern Ethiopia and Eritrea (mean value 0.87 Ga) and southern Ethiopia (1.13 Ga), respectively. Stern (2002) argued that these figures reflect dominantly Neoproterozoic mantle-derived melts, with a progressive influence of reworked pre-Mesoproterozoic crust southwards. In this context, the older model age of the Duksi complex, as compared to the 50 Ma younger Dogi batholith, can be taken to suggest also a temporal evolution towards a lesser influence of reworked crustal material through the closing stage of the 'Mozambique Ocean'. This is consistent with recent models for the assembly of Eastern Gondwana (Stern, 1994; Meert, 2003; Stern & Abdelsalam, 1998; Blasband *et al.* 2000) indicating that ocean closure was characterized by accretion of mainly juvenile, intraoceanic arc terranes between 750 and 650 Ma.

8. Conclusions

Combined geochronological, isotopic and chemical data indicate that the western Ethiopian shield contains major supracrustal and plutonic complexes that are indistinguishable from the southernmost parts of the Arabian–Nubian Shield in northern Ethiopia and Eritrea.

The earliest arc-related East African Orogen magmatism documented in western Ethiopia is dated at 866 ± 20 Ma (U–Pb zircon), which overlaps with a Rb–Sr whole-rock errorchron of 873 ± 82 Ma. It is represented by pyroclastic metavolcanites, dominated by basaltic andesite, that have the geochemical signatures of Andean-type high-K to medium-K calc-alkaline rocks. Positive ε_{Nd} values reflect the influence of a relatively thin and young continental crust. Interlayered basaltic flows are transitional to MORB and are interpreted to have formed in an extensional, back-arc or inter-arc, regime contemporaneous with active arc magmatism in a continental margin setting (Fig. 11). A related suite of dykes intrudes thick carbonate–psammite sequences of inferred pre-arc, continental shelf, origin. Ultramafic complexes in the region, previously interpreted as ophiolite fragments, are geochemically comparable to the sediment-hosted dykes and the metavolcanites, and probably represent solitary intrusions formed in response to limited arc extension. Combined with data elsewhere in the East African Orogen, the continental margin affinity of arc

https://doi.org/10.1017/S001675680300801X Published online by Cambridge University Press

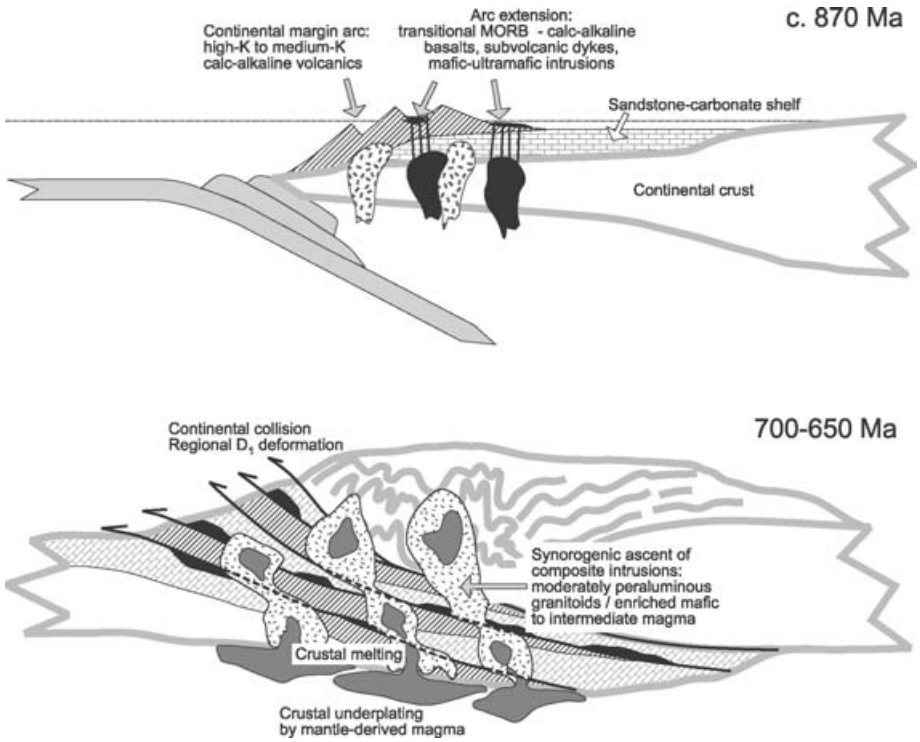

Figure 11. Schematic palaeotectonic model for the East African Orogen of Western Ethiopia. Subduction polarity is unknown and is arbitrarily drawn in the figure. For details, see discussion in text.

construction and rifting in western Ethiopia points to a possible southward increase in crustal thickness along the arc system in the early 'Mozambique Ocean'. Apparently, this corresponds with a decrease in the extent of marginal basin opening that led to the formation of ophiolites further north in the East African Orogen. Approximate analogues to this scenario can be found in the complex interplay of oceanic and continent-based arc construction, arc rifting and marginal basin spreading in the Sunda–Banda arc systems of Indonesia (Hamilton, 1979; Honthaas *et al.* 1998).

Synkinematic composite plutons have yielded crystallization ages of 699 ± 2 Ma (Duksi, U–Pb zircon) and 651 ± 5 Ma (Dogi, U–Pb titanite). They are characterized by abundant shoshonitic, latitic, trachytic and rare trachybasaltic intrusions with extreme enrichments of highly incompatible trace elements combined with positive ε_{Nd} values, thought to have formed by partial melting of enriched sub-continental mantle during the extensive collision phase of the East African Orogen (Fig. 11). Contemporaneous formation of moderately peraluminous granodiorites and granites with slightly positive ε_{Nd} values was related to crustal underplating of the mafic magmas and consequent melting of lower crustal material derived from the previously accreted, juvenile arc terranes of the East African Orogen.

Acknowledgements. This research was carried out under the auspices of the *Ethionor Program*, an institutional cooperation between the Geological Survey of Ethiopia (GSE) and the Geological Survey of Norway (NGU) funded by the Norwegian Agency for Development Cooperation (NORAD). We are grateful to Robert J. Stern and Jan D. Kramers for their thorough and constructive reviews of the manuscript, and to Abraham Amenti for discussions on the regional geology of Ethiopia. Elizabeth Eide is thanked for improving the English text. We would also like to express our thanks to Teweldebrhan Abay, Melese Getahun, Tesfaye Selato, Tekaligne Tesfaye, Ayele Wondimu, Ibrahim Yusuf, Wubshet Zewude and many other GSE geologists for sharing their knowledge of the local geology during the three field seasons of the project.

References

ABDELSALAM, M. G. & STERN, R. J. 1996. Sutures and shear zones in the Arabian–Nubian Shield. *Journal of African Earth Sciences* **23**, 289–310.

ALDANMAZ, E., PEARCE, J. A., THIRLWALL, M. F. & MITCHELL, J. G. 2000. Petrogenetic evolution of the Late Cenozoic, post-collision volcanism in western Anatolia, Turkey. *Journal of Volcanology and Geothermal Research* **102**, 67–95.

AYALEW, T., BELL, K., MOORE, J. M. & PARRISH, R. R. 1990. U–Pb and Rb–Sr geochronology of the Western Ethiopian Shield. *Geological Society of America Bulletin* **102**, 1309–16.

AYALEW, T. & PECCERILLO, A. 1998. Petrology and geochemistry of the Gore-Gambella plutonic rocks: implications for magma genesis and the tectonic setting of the Pan-African orogenic belt of western Ethiopia. *Journal of African Earth Sciences* **27**, 397–416.

BARBARIN, B. 1999. A review of the relationships between granitoid types, their origins and their geodynamic environments. *Lithos* **46**, 605–26.

https://doi.org/10.1017/S001675680300801X Published online by Cambridge University Press

BELLIENI, G., CAVAZZINI, G., FIORETTI, A. M., PECCERILLO, A. & ZANTEDESCHI, P. 1996. The Cima de Vila (Zinsnock) Intrusion, Eastern Alps: evidence for crustal melting, acid-mafic magma mingling and wall-rock fluid effects. *Mineralogy and Petrology* **56**, 125–46.

BERHE, S. M. 1990. Ophiolites in Northeast and East Africa: implications for Proterozoic crustal growth. *Journal of the Geological Society, London* **147**, 41–57.

BJERKGÅRD, T. 1997. *Geology in the Baruda, Galesa and Bulen areas, Western Ethiopia; preliminary results.* Norges geologiske undersøkelse, Report 97. 189, 49 pp.

BLASBAND, B., WHITE, S., BROOIJMANS, P., DE BOORDER, H. & VISSER, W. 2000. Late Proterozoic extensional collapse in the Arabian–Nubian Shield. *Journal of the Geological Society, London* **157**, 615–28.

BRAATHEN, A. & GRENNE, T. 1997. *Geology and mineralisation in the Baruda area, Metekel District, Gojam Province, Ethiopia: Preliminary results.* Norges geologiske undersøkelse, Report 97.116, 21 pp.

BRAATHEN, A., GRENNE, T., SELLASSIE, M. G. & WORKU, T. 2001. Juxtaposition of Neoproterozoic units along the Baruda – Tulu Dimtu shear belt in the East African Orogen of western Ethiopia. *Precambrian Research* **107**, 215–34.

CARN, S. A. & PYLE, D. M. 2001. Petrology and geochemistry of the Lamongan volcanic field, East Java, Indonesia: Primitive Sunda arc magmas in an extensional tectonic setting? *Journal of Petrology* **42**, 1643–83.

COLEMAN, R. G. 1977. *Ophiolites. Ancient oceanic lithosphere* ? Springer-Verlag, 229 pp.

DEMESSIE, M. 1996. *Bibliography of the geology of Ethiopia.* Ethiopian Institute of Geological Surveys, Occasional Publication 1996/33, 266 pp.

DE WIT, M. J. 1981. Precambrian base metals. In *Plate tectonics and metallogenesis: Some guidelines to Ethiopian mineral deposits* (eds S. Chewaka and M. J. de Wit), pp. 65–74. Ethiopian Institute of Geological Surveys Bulletin no. 2. Addis Ababa.

EWART, A., BRYAN, W. B., CHAPPELL, B. W. & RUDNICK, R. L. 1994. Regional geochemistry of the Lau-Tonga arc and backarc systems. *Proceedings of the Ocean Drilling Program, Scientific Results* **135**, 385–425.

GAMBLE, J. A., SMITH, I. E. M., MCCULLOCH, M. T., GRAHAM, I. J. & KOKELAAR, B. P. 1993. The geochemistry and petrogenesis of basalts from the Taupo volcanic zone and Kermadec island arc, S.W. Pacific. *Journal of Volcanology and Geothermal Research* **54**, 265–90.

GASS, I. G. 1990. Ophiolites and Oceanic Lithosphere. In *Ophiolites: Oceanic Crustal Analogues* (eds J. Malpas, E. M. Moores, A. Panayiotou and C. Xenophontos), pp. 1–10. Nicosia: Geological Survey Department and Ministry of Agriculture and Natural Resources.

GREEN, T. H. 1982. Anatexis of mafic crust and high pressure crystallization of andesite. In *Andesites; orogenic andesites and related rocks* (ed. R. S. Thorpe), pp. 465–87. Chichester: John Wiley & Sons.

GRENNE, T., BRAATHEN, A., SELASSIE, M. G. & WORKU, T. 1998. *Results and models from fieldwork in the Meso-Neoproterozoic belt of western Ethiopia: the Wembera-Baruda-Bulen-Kilaj transect of the Metekel Zone.* Norges geologiske undersøkelse, Report 98. 110, 51 pp.

HAWKESWORTH, C. J., NORRY, M. J., RODDICK, J. C., BAKER, P. E., FRANCIS, P. W. & THORPE, R. S. 1979. $^{143}Nd/^{144}Nd$, $^{87}Sr/^{86}Sr$, and incompatible element variations in calc-alkaline andesites and plateau lavas from South America: *Earth and Planetary Science Letters* **42**, 45–57.

HAMILTON, W. 1979. *Tectonics of the Indonesian Region.* U.S. Geoleological Survey Professional Paper 1078, 345 pp.

HONTHAAS, C., RÉHAULT, J. P., MAURY, R. C., BELLON, H., HÉMOND, C., MALOD, J. A., CORNÉE, J. J., VILLENEUVE, M., COTTEN, J., BURHANUDDIN, S., GUILLOU, H. & ARNAUD, N. 1998. A Neogene back-arc origin for the Banda Sea basins: geochemical and geochronological constraints from the Banda ridges (East Indonesia). *Tectonophysics* **298**, 297–317.

JENNER, G. A., LONGERICH, H. P., JACKSON, S. E. & FRYER, B. J. 1990. ICP-MS; a powerful tool for high-precision trace-element analysis in earth sciences; evidence from analysis of selected U.S.G.S. reference samples. *Chemical Geology* **83**, 133–48.

KAH, L. C., LYONS, T. W. & CHESLEY, J. T. 2001. Geochemistry of a 1.2 Ga carbonate-evaporite succession, northern Baffin and Bylot islands; implications for Mesoproterozoic marine evolution. *Precambrian Research* **111**, 203–34.

KAY, S. M., MPODOZIS, C., RAMOS, V. A. & MUNIZAGA, F. 1991. Magma source variations for mid-late Tertiary magmatic rocks associated with a shallowing subduction zone and a thickening crust in the Central Andes (28 to 33 °S). In *Andean Magmatism and its Tectonic Setting* (eds R. S. Harmon and C. W. Rapela), pp. 113–37. Geological Society of America, Special Paper no. 265.

KESKIN, M., PEARCE, J. A. & MITCHELL, J. G. 1998. Volcano-stratigraphy and geochemistry of collision-related volcanism on the Erzurum-Kars Plateau, northeastern Turkey. *Journal of Volcanology and Geothermal Research* **85**, 355–404.

KRÖNER, A. 1984. Late Precambrian plate tectonics and orogeny: a need to redefine the term Pan-African. In *African geology* (eds J. Klerkx and J. Michot), pp. 23–8. Tervuren: Musée R. L'Afrique Centrale.

KRÖNER, A., LINNEBACHER, P., STERN, R. J., REISCHMANN, T., MANTON, W. & HUSSEIN, I. M. 1991. Evolution of Pan-African island-arc assemblages in the southern Red-Sea Hills, Sudan, and in southwestern Arabia as exemplified by geochemistry and geochronology. *Precambrian Research* **53**, 99–118.

LE MAITRE, R. W., BATEMAN, P., DUDEK, A., KELLER, J., LEMEYRE, J., LE BAS, M. J., SABINE, P. A., SCHMID, R., SORENSEN, H., STRECKEISEN, A., WOOLEY, A. R. & ZANETTIN, B. 1989. *A classification of igneous rocks and glossary of terms. Recommendations of the International Union of Geological Sciences Subcommision on the Systematics of Igneous Rocks.* Oxford: Blackwell Scientific Publishers, 193 pp.

LONGERICH, H. P., JENNER, G. A., FRYER, B. J. & JACKSON, S. E. 1990. Inductively coupled plasma-mass spectrometric analysis of geological samples; a critical evaluation based on case studies. *Chemical Geology* **83**, 105–18.

LÒPEZ-ESCOBAR, L., TAGIRI, M. & VERGARA, M. 1991. Geochemical features of Southern Andes Quaternary volcanics between 41°50′ and 43°00′S. In *Andean Magmatism and its Tectonic Setting* (eds R. S. Harmon and C. W. Rapela), pp. 45–56. Geological Society of America, Special Paper no. 265.

LUDWIG, K. R. 1980. Calculations of uncertainties of U–Pb isotope data. *Earth and Planetary Science Letters* **46**, 212–20.

https://doi.org/10.1017/S001675680300801X Published online by Cambridge University Press

MACLACHLAN, K. & DUNNING, G. 1998. U–Pb ages and tectonomagmatic relationships of early Ordovician low-Ti tholeiites, boninites and related plutonic rocks in central Newfoundland, Canada. *Contribution to Mineralogy and Petrology* **133**, 235–58.

MCBIRNEY, A. R. 1993. *Igneous Petrology.* Boston, London: Jones and Bartlett Publishers, 508 pp.

MEERT, J. G. 2003. A synopsis of events related to the assembly of eastern Gondwana. *Tectonophysics* **362**, 1–40.

MILLER, C. A., BARTON, M., HANSON, R. E. & FLEMING, T. H. 1994. An Early Cretaceous volcanic arc marginal basin transition zone, Peninsula Hardy, Southernmost Chile. *Journal of Volcanology and Geothermal Research* **63**, 33–58.

NELSON, B. K. & DEPAOLO, D. J. 1985. Rapid production of continental crust 1.7 to 1.9 b.y. ago: Nd isotopic evidence from the basement of the North American mid-continent. *Geological Society of America Bulletin* **96**, 746–54.

NICOLAS, A. 1989. *Structures of Ophiolites and Dynamics of Oceanic Lithosphere.* Dordrecht, Boston, London: Kluwer Academic Publishers, 367 pp.

NOHDA, S. & WASSERBURG, G. J. 1981. Nd and Sr isotopic study of volcanic rocks from Japan. *Earth and Planetary Science Letters* **52**, 264–76.

PEARCE, J. A. 1983. Role of the sub-continental lithosphere in magma genesis at active continental margins. In *Continental basalts and mantle xenoliths* (eds C. J. Hawkesworth and M. J. Norry), pp. 230–49. Nantwich: Shiva.

PEARCE, J. A., BAKER, P. E., HARVEY, P. K. & LUFF, I. W. 1995*b*. Geochemical evidence for subduction fluxes, mantle melting and fractional crystallization beneath the South Sandwich-island arc. *Journal of Petrology* **36**, 1073–1109.

PEARCE, J. A., BENDER, J. F., DE LONG, S. E., KIDD, W. S. F., LOW, P. J., GÜNER, Y., SAROGLU, F., YILMAZ, Y., MOORBATH, S. & MITCHELL, J. G. 1990. Genesis of collision volcanism in Eastern Anatolia, Turkey. *Journal of Volcanology and Geothermal Research* **44**, 189–229.

PEARCE, J. A., ERNEWEIN, M., BLOOMER, S. H., PARSON, L. M., MURTON, B. J. & JOHNSON, L. E. 1995*a*. Geochemistry of Lau Basin volcanic rocks: influence of ridge segmentation and arc proximity. In *Volcanism Associated with Extension at Consuming Plate Margins* (ed. J. L. Smellie), pp. 53–75. Geological Society of London, Special Publication no. 81.

PEARCE, J. A., HARRIS, N. B. W. & TINDLE, A. G. 1984. Trace element discrimination diagrams for the tectonic identification of granitic rocks. *Journal of Petrology* **25**, 956–83.

PEARCE, J. A. & PARKINSON, I. J. 1993. Trace element models for mantle melting; application to volcanic arc petrogenesis. In *Magmatic processes and plate tectonics* (eds H. M. Prichard, T. Alabaster, N. B. W. Harris and C. R. Neary), pp. 373–403. Geological Society of London, Special Publication no. 76.

PEARCE, J. A. & PEATE, D. W. 1995. Tectonic implications of the composition of volcanic arc magmas. *Annual Review of Earth and Planetary Sciences* **23**, 251–85.

PETFORD, N. & ATHERTON, M. P. 1995. Cretaceous–Tertiary volcanism and syn-subduction crustal extension in northern central Peru. In *Volcanism Associated with Extension at Consuming plate Margins* (ed. J. L. Smellie), pp. 233–48. Geological Society of London, Special Publication no. 81.

PIN, C., BRIOT, D., BASSIN, C. & POITRASSON, F. 1994. Concomitant separation of strontium and samarium–neodynium for isotope analyses in silicate samples, based on specific extraction chromatography. *Analytica Chimica Acta* **298**, 209–17.

POUCLET, A., LEE, J. S., VIDAL, P., COUSENS, B. & BELLON, H. 1995. Cretaceous to Cenozoic volcanism in South Korea and in the Sea of Japan: magmatic constraints on the opening of the back-arc basin. In *Volcanism Associated with Extension at Consuming plate Margins* (ed. J. L. Smellie), pp. 169–91. Geological Society of London, Special Publication no. 81.

RIGGS, N. R. & BUSBY-SPERA, C. J. 1990. Evolution of a multivent volcanic complex within a subsiding arc graben depression – Mount-Wrightson Formation, Arizona. *Geological Society of America Bulletin* **102**, 1114–35.

SAUNDERS, A. D., TARNEY, J., KERR, A. C. & KENT, R. W. 1996. The formation and fate of large oceanic igneous provinces. *Lithos* **37**, 81–95.

STACEY, J. S. & KRAMERS, J. D. 1975. Approximation of terrestrial lead isotope evolution by a two-stage model. *Earth and Planetary Science Letters* **26**, 207–21.

STEIN, M. & GOLDSTEIN, S. L. 1996. From plume head to continental lithosphere in the Arabian–Nubian Shield. *Nature* **382**, 773–8.

STERN, R. J. 1994. Arc assembly and continental collision in the Neoproterozoic East African orogen. *Annual Review of Earth and Planetary Sciences* **22**, 319–51.

STERN, R. J. 2002. Crustal evolution in the East African Orogen, a neodymium isotopic perspective. *Journal of African Earth Sciences* **34**, 109–17.

STERN, R. J. & ABDELSALAM, M. G. 1998. Formation of juvenile continental crust in the Arabian–Nubian shield: evidence from granitic rocks of the Nakasib suture, NE Sudan. *Geologische Rundschau* **87**, 150–60.

STERN, R. J. & HEDGE, C. E. 1985. Geochronologic and isotopic constraints on late Precambrian crustal evolution in the Eastern Desert of Egypt. *American Journal of Science* **285**, 97–127.

SUN, S. S. & MCDONOUGH, W. F. 1989. Chemical and isotopic systematics of oceanic basalts: implications for mantle compositions and processes. In *Magmatism in ocean basins* (eds A. D. Saunders and M. J. Norry), pp. 313–45. Geolological Society of London, Special Publication no. 42.

TADESSE, T., HOSHINO, M. & SAWADA, Y. 1999. Geochemistry of low-grade metavolcanic rocks from the Pan-African of the Axum area, northern Ethiopia. *Precambrian Research* **99**, 101–24.

TADESSE, T., HOSHINO, M., SUZUKI, K. & SHIGERU, I. 2000. Sm–Nd, Rb–Sr and Th–U Pb zircon ages of syn- and post-tectonic granitoids from the Axum area of northern Ethiopia. *Journal of African Earth Sciences* **30**, 313–27.

TAMAKI, K. 1995. Opening tectonics of the Japan Sea. In *Back-arc basins: tectonics and magmatism* (ed. B. Taylor), pp. 407–20. New York: Plenum Press.

TEFERA, M. 1991. *Geology of the Kurmuk and Asosa area. Preliminary report.* Ethiopian Institute of Geological Surveys, 112 pp.

TEFERA, M. 1997. *Bedrock map Kurmuk and Asosa, M 1:250000.* Ethiopian Institute of Geological Surveys.

TEKLAY, M. 1997. *Petrology, geochemistry and geochronology of Neoproterozoic magmatic arc rocks from Eritrea:*

Implications for crustal evolution in the southern Nubian Shield. Memoir 1, Department of Mines, Eritrea, 125 pp.

TEKLAY, M., KRÖNER, A. & MEZGER, K. 2002. Enrichment from plume interaction in the generation of Neoproterozoic arc rocks in northern Eritrea: implications for crustal accretion in the southern Arabian–Nubian Shield. *Chemical Geology* **184**, 167–84.

TEKLAY, M., KRÖNER, A., MEZGER, K. & OBERHÄNSLI, R. 1998. Geochemistry, Pb–Pb single zircon ages and Nd–Sr isotope composition of Precambrian rocks from southern and eastern Ethiopia: implications for crustal evolution in East Africa. *Journal of African Earth Sciences* **26**, 207–27.

TORMEY, D. R., HICKEY-VARGAS, R., FREY, R. A. & LOPEZ-ESCOBAR, L. 1991. Recent lavas from the Andean volcanic front (33–42°S); interpretations of along-arc compositional variations. In *Andean Magmatism and its Tectonic Setting* (eds R. S. Harmon and C. W. Rapela), pp. 57–77. Geological Society of America, Special Paper no. 265.

UJIKE, O. & TSUCHIYA, N. 1993. Geochemistry of Miocene basaltic rocks temporally straddling the rifting of lithosphere at the Akita–Yamagata area, Northeast Japan. *Chemical Geology* **104**, 61–74.

VERGARA, M., LEVI, B., NYSTRÖM, J. O. & CANCINO, A. 1995. Jurassic and Early Cretaceous island arc volcanism, extension, and subsidence in the Coast Range of central Chile. *Geological Society of America Bulletin* **107**, 1427–40.

VROON, P. Z., VANBERGEN, M. J., WHITE, W. M. & VAREKAMP, J. C. 1993. Sr–Nd–Pb isotope systematics of the Banda Arc, Indonesia – combined subduction and assimilation of continental material. *Journal of Geophysical Research* **98**, 22349–66.

WILSON, M. 1989. *Igneous petrogensis – a global tectonic approach.* London: Chapman & Hall, 466 pp.

WORKU, H. & SCHANDELMEIER, H. 1996. Tectonic evolution of the Neoproterozoic Adola Belt of southern Ethiopia: evidence for a Wilson Cycle process and implications for oblique plate collision. *Precambrian Research* **77**, 179–210.

https://doi.org/10.1017/S001675680300801X Published online by Cambridge University Press